Article

Cell

Compartmentalization of a Bistable Switch Enables Memory to Cross a Feedback-Driven Transition

Graphical Abstract

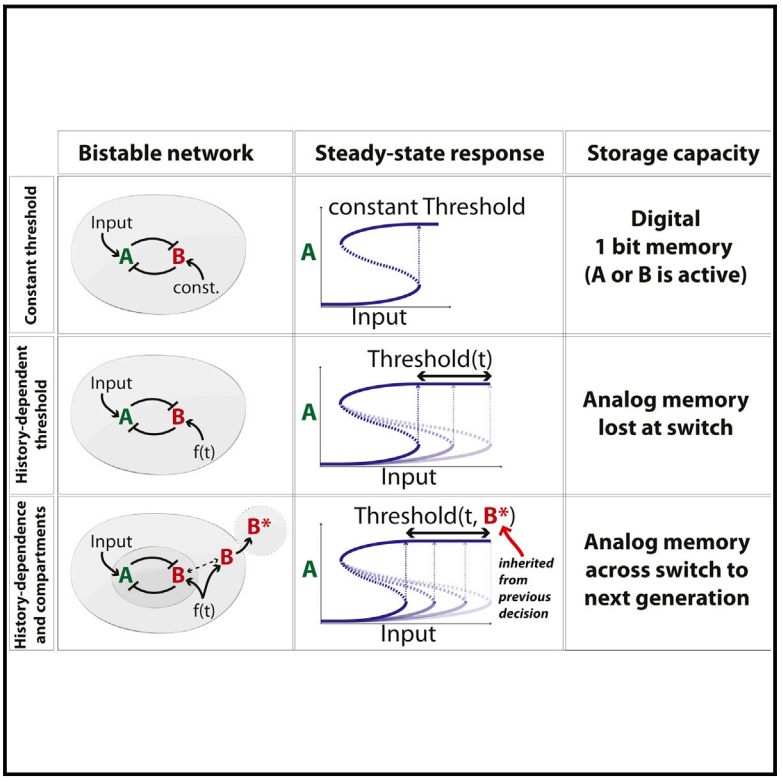

Authors

Andreas Doncic, Oguzhan Atay, ..., Mart Loog, Jan M. Skotheim

Correspondence

skotheim@stanford.edu

In Brief

The spatial organization of the G1/S switch enables the intergenerational transmission of memory of pheromone exposure in budding yeast.

Highlights

- Yeast decide to enter the cell cycle based on the history of pheromone exposure
- Compartmentalization enables transmission of memory from mother to daughter
- Intergenerational memory of pheromone exposure is stored as cytoplasmic Far1
- Anchoring of cytoplasmic Far1 by Cdc24 is required for intergenerational memory

Doncic et al., 2015, Cell *160*, 1182–1195
March 12, 2015
http://dx.doi.org/10.1016/j.cell.2015.02.032

CellPress

Cell

Article

Compartmentalization of a Bistable Switch Enables Memory to Cross a Feedback-Driven Transition

Andreas Doncic,[1] Oguzhan Atay,[1] Ervin Valk,[2] Alicia Grande,[3] Alan Bush,[3] Gustavo Vasen,[3] Alejandro Colman-Lerner,[3] Mart Loog,[2] and Jan M. Skotheim[1,*]

[1]Department of Biology, Stanford University, Stanford, CA 94305, USA

[2]Institute of Technology, University of Tartu, 50411, Estonia

[3]IFIBYNE-UBA-CONICET and Departamento de Fisiología, Biología Molecular y Celular, Facultad de Ciencias Exactas y Naturales, Universidad de Buenos Aires, Buenos Aires C1428EHA, Argentina

*Correspondence: skotheim@stanford.edu

http://dx.doi.org/10.1016/j.cell.2015.02.032

SUMMARY

Cells make accurate decisions in the face of molecular noise and environmental fluctuations by relying not only on present pathway activity, but also on their memory of past signaling dynamics. Once a decision is made, cellular transitions are often rapid and switch-like due to positive feedback loops in the regulatory network. While positive feedback loops are good at promoting switch-like transitions, they are not expected to retain information to inform subsequent decisions. However, this expectation is based on our current understanding of network motifs that accounts for temporal, but not spatial, dynamics. Here, we show how spatial organization of the feedback-driven yeast G1/S switch enables the transmission of memory of past pheromone exposure across this transition. We expect this to be one of many examples where the exquisite spatial organization of the eukaryotic cell enables previously well-characterized network motifs to perform new and unexpected signal processing functions.

INTRODUCTION

Cellular signaling pathways are used to transmit information about the extra- and intra-cellular environment. Specific outputs from such signaling pathways are then used by decision-making networks to determine cellular response. Currently, signaling pathways are most often described as static schematics based on a combination of genetic dependencies and biochemical interactions. While a good first step, such a characterization can neither describe nor predict the pathway dynamics that determine cellular response to time-dependent input signals (Behar et al., 2008; Yosef and Regev, 2011). Indeed, outputs of the regulatory networks controlling proliferation and apoptosis depend on the history of dynamic input signals, not only on current levels (Doncic and Skotheim, 2013; Lee et al., 2012; Purvis et al., 2012). This strongly suggests that the ability to retain information from prior states is a key determinant informing cellular decision making.

Signaling dynamics play important roles in many networks regulating switch-like transitions between distinct states. The switch-like nature of transitions often arises from positive feedback loops that quickly increase the activity of key regulatory proteins when triggered by input signals above a specific threshold. Networks containing positive feedback loops frequently give rise to bistability, i.e., for a range of input signals, the output will be one of two possible values depending on the history of the input signal. However, this is a very simple form of history dependence as all possible time-dependent input signals get mapped onto only two possible outputs, i.e., history dependence is collapsed onto only a single bit of information. This implies that while positive feedback loops may be good at promoting switch-like transitions, they appear unable to retain more than rudimentary information about signaling pathway history. It is therefore improbable that a positive-feedback-driven switch can be used to transmit information to inform future cellular decisions. However, this conclusion is based on the current framework for analyzing network motifs such as feedback-loops or feed-forward interactions (Alon, 2007), which accounts for temporal but not spatial dynamics. Thus, while it is well-known that spatial organization plays an important role in signal transduction, we do not currently know how or if the eukaryotic cell's spatial organization can affect existing motif functions or give rise to entirely new motif functions (Howell et al., 2012; Kholodenko et al., 2010; Santos et al., 2012).

To better understand how spatial organization might affect cellular signal processing, we decided to examine the cell-cycle control network responsible for the decision to divide in budding yeast. In yeast, the decision to commit to cell division takes place in late G1, prior to DNA replication at a point called *Start* (Hartwell et al., 1974). Multiple internal and external signals are integrated to determine when a cell passes *Start*, beyond which cells no longer respond to mating pheromone (α-factor). *Start* is a switch-like, irreversible transition that corresponds to the activation of a positive feedback loop of cyclin-dependent kinase (Cdk1) activity (Doncic et al., 2011). Specifically, Cln3-Cdk partially inactivates Whi5, a transcriptional inhibitor of the expression of the G1 cyclins *CLN1* and *CLN2*. The expression of Cln1 and Cln2 complete inactivation of Whi5 by forming a positive feedback loop (Costanzo et al., 2004; de Bruin et al., 2004; Skotheim et al., 2008).

Prior to *Start*, cells can be arrested by pheromone-dependent activation of the mitogen activated protein kinase (MAPK) mating pathway (Chen and Thorner, 2007). Upon pheromone exposure, the MAPK Fus3 phosphorylates and activates the Cdk inhibitor Far1, which inhibits the G1 cyclins essential for progression through *Start* (Chang and Herskowitz, 1990; Gartner et al., 1998; Jeoung et al., 1998; Peter et al., 1993; Pope et al., 2014; Tyers and Futcher, 1993). Conversely, post-*Start*, the G1 cyclins inhibit the mating pathway by targeting the upstream scaffold protein Ste5 as well as Far1 (Garrenton et al., 2009; Henchoz et al., 1997; Peter and Herskowitz, 1994; Strickfaden et al., 2007; Tyers and Futcher, 1993) (Figure S1A). Thus, progression through *Start* drives an increase in cyclin expression that results in Far1 degradation, whereas pre-*Start* exposure to pheromone leads to Far1 activation, G1 cyclin inhibition, and G1 arrest (Doncic et al., 2011; McKinney et al., 1993; Pope et al., 2014). In other words, the regulatory network underlying *Start* is bistable, where a well-defined commitment point separates stable low- and high-Cdk activity states, and only the low-Cdk activity state can be inhibited by MAPK signaling (Doncic et al., 2011).

Although this characterization of *Start* is accurate for a step input of high pheromone concentration, cells exposed to low or intermediate pheromone concentrations do not arrest permanently, but rather delay progression through G1 (Hao et al., 2008; Malleshaiah et al., 2010; Moore, 1984). This suggests a more complex decision making machinery that balances the benefits of successful mating with the costs of staying arrested and both failing to mate and proliferate. Thus, while the *Start* network remains bistable, its output changes from a digital response to arrest or not, to an analog computation determining how long to arrest before reentering the cell division cycle. We previously showed that in this analog computation, yeast cells decide to reenter the cell cycle based on their history of exposure to pheromone during an arrest, not just the current pathway activity (Doncic and Skotheim, 2013). Time-dependent pheromone signals are processed by the MAPK pathway using a coherent feed-forward motif in which the MAPK Fus3 activates Far1 both by direct phosphorylation and by increasing its expression via the Ste12 transcription factor (Chang and Herskowitz, 1990; Errede and Ammerer, 1989; Gartner et al., 1998) (Figure S1A; red arrows). This architecture allows a robust yet rapidly reversible cellular state. Far1 accumulates to provide a memory so that cells exposed to pheromone for longer durations have more Far1 rendering them more reluctant to reenter the cell cycle. In addition, fast dephosphorylation allow Far1 to be rapidly inactivated so that cells can rapidly reenter the cell cycle if the MAPK signal plummets (Doncic and Skotheim, 2013).

Although the accumulation of Far1 provides a mechanism to remember the history of pheromone exposure during a single arrest, it does not suggest a mechanism to transmit this information to subsequent generations after cell-cycle reentry. This is because the mutual inhibition of Cdk and Far1 activity underlying the bistable *Start* switch is expected to target all Far1 for degradation once the cell cycle has been reentered. Similarly, the sharp switch at mitotic exit also employs ultra-sensitive protein degradation (Yang and Ferrell, 2013). Protein degradation may be useful to sharpen switches and reset regulatory circuits, but comes at the cost of losing cellular memory. Thus, while bistable regulatory networks are excellent at generating all-or-none transitions, they limit the amount of information that can be propagated across these transitions.

Here, we show how compartmentalization of the bistable G1 control network allows cellular memory to traverse the *Start* switch. Far1 is split into nuclear and cytoplasmic pools that combat distinct sets of cyclin-Cdk complexes allowing these two compartments of the Far1-Cdk switch to have distinct dynamics. Upon reentering the cell cycle from pheromone arrest, nuclear Far1 is rapidly degraded, while cytoplasmic Far1 is degraded much more slowly so that a substantial pool remains at the beginning of the next division cycle. We show that this inherited pool contributes to cell-cycle arrest in the daughter cells so that the mother cells are able to transmit their memory of pheromone exposure to the next generation. This intergenerational memory depends on the anchoring of Far1 to cytoplasmic Cdc24, a regulator of cell polarization. Thus, we demonstrate how compartmentalization of a bistable regulatory circuit enables an entirely new function to be performed by this well-characterized signaling motif. More broadly, our results argue that spatial organization can greatly enhance the function of regulatory motifs and is therefore just as integral to pathway function as network topology and chemical kinetics.

RESULTS

Nuclear Far1 and Nuclear Cln2 Function in Cell-Cycle Commitment

To determine if and how signal information could be propagated across a bistable switch, we examined the network regulating *Start*, the point of commitment to cell division in budding yeast (Figure 1A). Since cyclin-Cdk complexes phosphorylate Far1 to target it for degradation, we expected that Far1 would be rapidly degraded upon progression through *Start*.

To examine the localization and dynamics of Far1, we used a Far1-Venus fusion protein expressed from the endogenous locus (Figure 1B). This *FAR1-Venus* strain exhibited the same arrest kinetics as an unlabeled WT strain, and we will subsequently refer to *FAR1-Venus* strains as WT (Doncic and Skotheim, 2013). Unless specified otherwise, all strains are in a background lacking the Bar1 protease that cleaves mating pheromone (for strain and plasmid lists see Table S1 and Table S2). Cells were arrested in high pheromone (240 nM α-factor) and released into pheromone-free medium using a previously described microfluidics-based assay (Doncic et al., 2011). Consistent with previous results (McKinney et al., 1993), Far1 was synthesized during mating arrest and mostly degraded post-*Start* after release into pheromone-free medium. However, the examination of Far1-Venus using time-lapse microscopy revealed a striking spatial dichotomy in Far1 degradation kinetics. The nuclear pool of Far1 is rapidly degraded in less than 10 min (approximately 7 min after *Start*), which is defined as when 50% of Whi5 has been exported from the nucleus (Doncic et al., 2011). Nuclear Far1 is degraded at approximately the same time as the Cdk-B-type cyclin inhibitor Sic1, which we previously measured as occurring ~8 min after *Start* (see Figures S1B and S1C for Far1 degradation

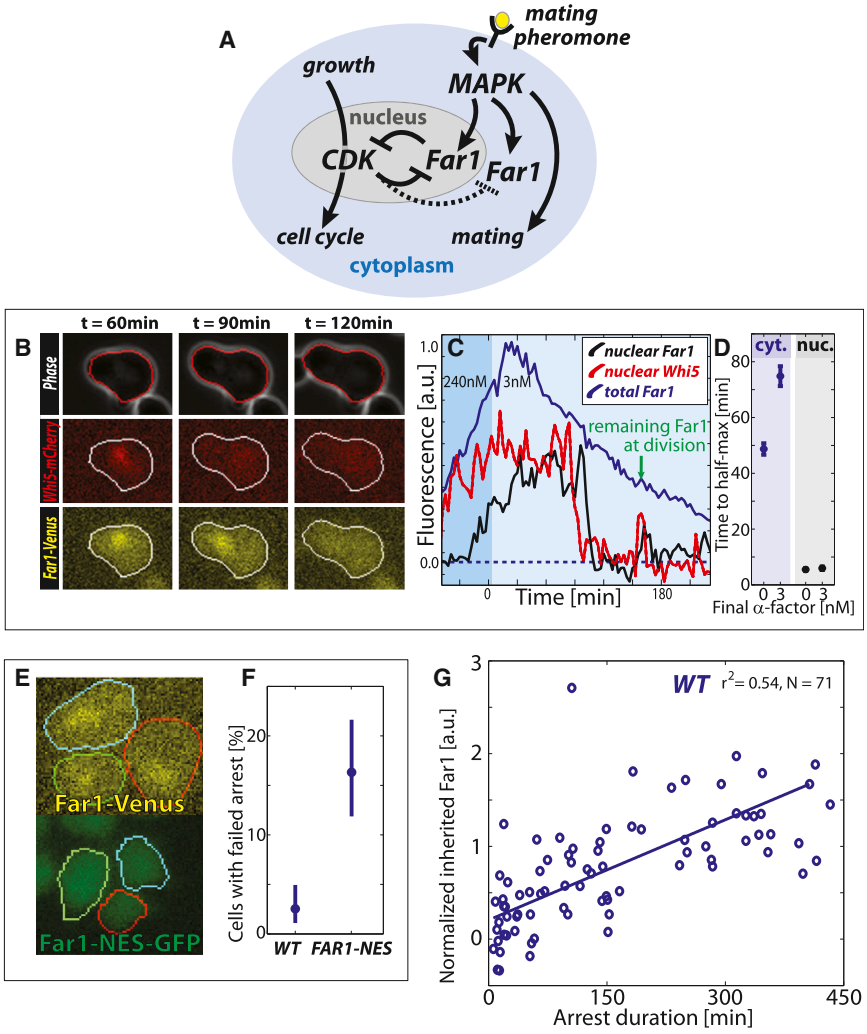

Figure 1. Cytoplasmic Far1 Is Inherited to Provide Intergenerational Memory across the *Start* Switch

(A) Schematic of the double-negative feedback (equivalent to positive feedback) network that regulates the switch between cell-cycle progression and pheromone arrest.

(B) Example images of segmented phase, Whi5-mCherry (red) and Far1-Venus (yellow) channels for cells reentering the cell cycle. Whi5-mCherry is nuclear in arrested cells.

(C) Example time series of nuclear Whi5-mCherry, and nuclear and cytoplasmic Far1-Venus that corresponds to the cell shown in (B). Nuclear Far1 is much more rapidly degraded than cytoplasmic Far1.

(D) Time from peak to half-maximum for cytoplasmic and nuclear Far1 in cells arrested in 240 nM and released into either 3 or 0 nM pheromone.

(E) Example *FAR1-Venus* and *FAR1-NES-GFP* cells arrested in 240 nM for 2 hr show that the nuclear localization is diminished in the *FAR1-NES-GFP* cells.

(F) A larger fraction of pre-*Start FAR1-NES* cells fails to arrest when abruptly exposed to 240 nM pheromone, where *Start* is defined as removal of 50% of nuclear Whi5-mCherry.

(G) Inherited Far1 in daughter cells is correlated with arrest duration.

Error bars in (D) denote SEM, while error bars in (F) denote 95% confidence intervals from 10,000 bootstrap iterations.

timing and (Doncic et al., 2011) for Sic1 degradation timing). This implies that Far1 degradation is likely coincident with the appearance of B-type cyclin activity in the nucleus. However, the cytoplasmic pool lingered and reached half-maximum ~50 min after *Start* (Figures 1C and 1D). This observed difference in Far1 degradation kinetics may be due to the nuclear F-box protein Cdc4 that mediates Far1 degradation (Blondel et al., 2000). This demonstrates that there are two separate pools of Far1 protein being degraded on very different time scales.

The rapid degradation of nuclear Far1 upon progression through *Start* suggests that it is primarily this nuclear pool that contributes to the commitment decision in response to exposure to pheromone (Blondel et al., 1999; Blondel et al., 2000). To test this, we added a nuclear export sequence to the endogenous *FAR1* allele (*FAR1-NES*), which greatly reduced the nuclear pool without affecting expression levels (Figures 1E and S1D). We then examined the cellular response to an abrupt increase in pheromone in the framework we previously developed to examine *Start* (Doncic et al., 2011). When exposed to a step-increase of pheromone, pre-*Start FAR1-NES* cells were over six times more likely than WT cells to fail to arrest despite not having traversed the Whi5-threshold (16% *FAR1-NES* versus 2.5% WT, Figure 1F). In addition, we found that nuclear, but not cytoplasmic Cln2 participated in *Start* (Figures S1E–S1I). Taken together, these results support a role for nuclear Far1 in *Start*.

Cytoplasmic Far1 Provides Intergenerational Memory of Pheromone Exposure

Even though nuclear Far1 was important for *Start*, most Far1 in arrested cells (~90%) is cytoplasmic and is not degraded rapidly upon cell-cycle reentry (Figures S2A–S2E). In fact, cytoplasmic Far1 is so slowly degraded after cell-cycle reentry that appreciable quantities are passed on to subsequent generations (Figures 1C and S2F). This is surprising because once cells reenter the cell cycle, these mother cells are desensitized to that level of pheromone and divide repeatedly without delay (Figure S2G) (Caudron and Barral, 2013; Doncic and Skotheim, 2013; Moore, 1984). To examine the role of inherited Far1 in daughter cells, we briefly arrested cells at high pheromone concentration (240 nM) before releasing the cells into an intermediate pheromone concentration (3 nM). The time to reach half-maximum Far1 post-*Start* in 3 nM pheromone was ~5 min in the nuclear pool and ~75 min in the cytoplasmic pool (Figure 1D). Thus, the time to reach cytoplasmic half-maximum post-*Start* is

increased relative to cells reentering in pheromone-free medium. Consequently, daughter cells entering the cell cycle in 3 nM pheromone inherited an increased amount of Far1 compared to daughter cells entering the cell cycle in pheromone-free medium (Figure S2H). This finding, that cells cycling in higher pheromone concentrations pass increasing amounts of Far1 on to their daughter cells, led us to hypothesize that inheritance of cytoplasmic Far1 is the molecular basis of an *intergenerational memory* of pheromone exposure.

To test the *intergenerational memory* hypothesis, we measured both the amount of inherited Far1 and subsequent G1 duration for daughter cells cycling in 3 nM, an intermediate mating pheromone concentration (see Experimental Procedures and Figure S2I). The more Far1 a daughter cell inherited, the longer it delayed progression through G1, supporting the hypothesis that mother cells transmit information about pheromone exposure to their daughters through cytoplasmic Far1 (Figure 1G). We also examined if differential inheritance of MAPK pathway scaffold Ste5, which affects pheromone signaling in a dosage-dependent manner (Thomson et al., 2011), could affect arrest duration, but found no effect (Figure S2J and S2K).

Compartmentalization Is Supported by a Fixed Fraction of Cytoplasmic Far1

The rapid degradation of the nuclear, but not cytoplasmic pool of Far1, requires a slow exchange between these two pools. Indeed, it would be impossible to maintain Far1 post-*Start* if Far1 were exchanged rapidly between the two pools as the half-life of nuclear Far1 is ~5 min. To investigate this requirement, we photobleached the nucleus of *FAR1-Venus* cells and measured the recovery of nuclear fluorescence (Figure 2A). Pre-*Start* cells were identified by examining the localization of Whi5-mKO fusion proteins expressed from the endogenous locus. After photobleaching, a significant recovery of the nuclear fraction on the 10 s timescale was seen. However, the nuclear to cytoplasmic fluorescence ratio did not recover to its initial level and reached a plateau prior to 30 s (Figures 2B–2D). Note that there is little new protein synthesis or degradation over the time frame of the experiment so that nearly all the recovery is due to protein translocation. The incomplete recovery of the nuclear-to-cytoplasmic ratio of Far1-*Venus* indicates that there is a pool of Far1 molecules that does not shuttle between the nucleus and the cytoplasm. As a control, we examined recovery of the yellow fluorescent protein YFP expressed from an *ACT1* promoter. The YFP nuclear-to-cytoplasmic ratio completely recovered after bleaching, which is consistent with rapid and unencumbered shuttling between nucleus and cytoplasm (Figure 2D). Taken together, we here identify both a rapidly shuttling and a fixed pool of Far1, which supports our model for how compartmentalization is used to generate intergenerational memory.

To transmit intergenerational memory, there should be a fixed cytoplasmic pool of Far1. While a single FRAP experiment indicates the presence of a fixed Far1 pool, it does not identify its location. To determine if there is fixed Far1 in the cytoplasm, we photobleached the nucleus four times sequentially and measured depletion of cytoplasmic Far1-Venus or YFP (Figures 2E and 2F). In the case of YFP, there is no fixed pool, so that the nuclear-to-cytoplasmic ratio recovers after each photobleaching event. Thus, each bleaching of the nucleus bleaches a constant fraction of the total protein. This leads to a linear relationship between the logarithm of the fluorescence and the number of photobleaching events (see Supplemental Information). A fixed cytoplasmic pool would result in a deviation from this linear fit. To test for a fixed cytoplasmic pool, we fit the normalized logarithm of the cytoplasmic fluorescence to a quadratic equation for each cell (Figure 2G). We find positive quadratic coefficients for Far1-Venus fits indicating the presence of a pool of Far1 that is fixed in the cytoplasm (Figure 2H).

Pheromone Exposure Is Remembered across the Entire Cell Cycle

To better understand intergenerational memory, we sought to investigate the mechanisms responsible for the increased time to half-maximum concentration of Far1 in 3 nM relative to 0 nM pheromone (Figure 1D). Such an increase could arise due to either increased Far1 synthesis or decreased Far1 degradation, or both. To test for regulated protein degradation, we expressed a *FAR1-Venus* fluorescent fusion protein from a galactose-inducible *GAL1* promoter. We inactivated Far1 synthesis by switching the carbon source from galactose to glucose and measured Far1 half-life post-*Start* (Figure 3A). Far1 stability post-*Start* is only weakly sensitive to pheromone concentration, which suggests that continued synthesis is more likely than increased protein stability to underlie increased inheritance of cytoplasmic Far1 at intermediate pheromone concentrations (Figures 3B and S4A). To test this possibility, we used single molecule fluorescence in situ hybridization (smFISH) (Raj et al., 2008), to measure the amount of *FAR1* mRNA transcripts (Figure 3C). Indeed, *FAR1* transcription was higher in 3 nM compared to 0 nM for cells with small and medium sized buds, corresponding to S and G2 cells respectively (Figures 3D). For large budded cells, likely about to divide, the number of *FAR1* transcripts was similarly high for both conditions, consistent with previous work showing that *FAR1* and other Ste12 transcription factor targets are transcribed at the M/G1 transition, even at 0 nM pheromone (Doncic and Skotheim, 2013; McKinney et al., 1993; Oehlen et al., 1996).

To test if the increased Far1 transcription in intermediate pheromone concentrations results from MAPK pathway activity, we examined *STE5-YFP* cells expressing the mating pathway scaffold protein Ste5 fused to a yellow fluorescent protein (Yu et al., 2008). Ste5 localizes to the site of polarized growth when the mating pathway is active (Pryciak and Huntress, 1998; Strickfaden et al., 2007). *STE5-YFP* cells were arrested in 3 nM pheromone and tracked through a cell cycle. The cell perimeter was segmented, linearized, and plotted on a kymograph to visualize the location and intensity of Ste5-YFP on the cell membrane (Figures 3E and 3F). As expected, we observed a transition from a low to a high level of Ste5-YFP at the site of polarized growth upon pheromone arrest (Figure 3G). Upon reentering the cell cycle, Ste5-YFP only partially dissociates from the membrane suggesting that the MAPK pathway remains active through the cell cycle at intermediate pheromone concentrations ($p < 0.05$ for all comparisons, Figure 3H). We

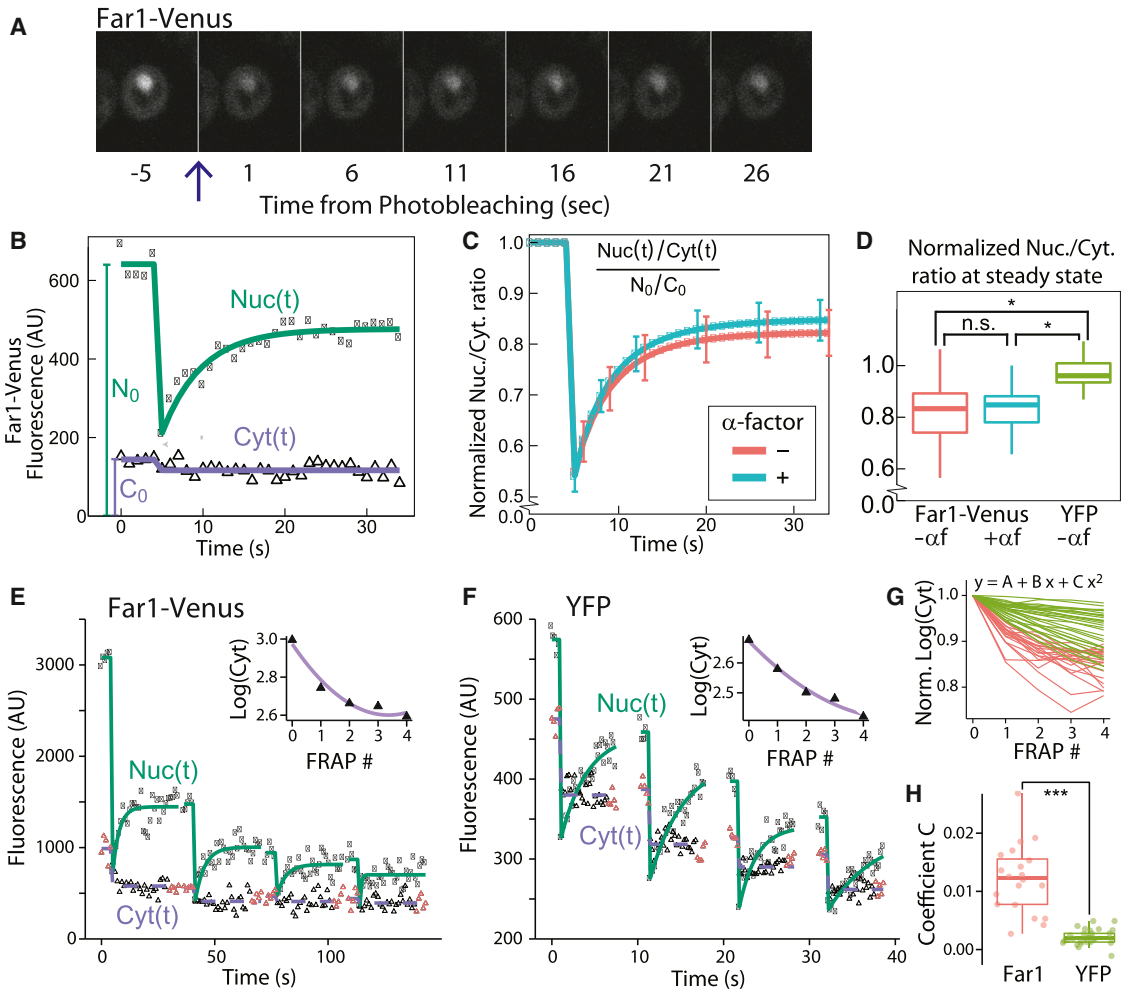

Figure 2. A Pool of Far1 Is Fixed in the Cytoplasm

(A) Fluorescence images from a typical time course, where the nuclear Far1-Venus was photobleached at t = 0.

(B) Data and model fit for nuclear, *Nuc(t)*, and cytoplasmic, *Cyt(t)*, Far1. N_0 and C_0 denote the initial nuclear and cytoplasmic fluorescence.

(C) Mean nuclear-to-cytoplasmic ratio of Far1-Venus normalized to its initial value, N_0/C_0. Bars denote the 95% confidence interval of the mean. We examined pre-*Start* G1 cells either not exposed to α-factor (red) or exposed to 500 nM α-factor (blue).

(D) Distribution of the estimated steady-state value of the normalized Nuc/Cyt ratio after photobleaching. Cells expressing Far1-Venus (blue/red) do not recover the initial nuclear-to-cytoplasmic ratio, while cells expressing the fluorescent protein YFP from an integrated ACT1 promoter (green) recover the initial ratio (see also Figure S3).

(E and F) Nuclear and cytoplasmic fluorescence from Far1-Venus or YFP following four sequential photobleaching events. Inset shows logarithm base 10 of the mean steady-state cytoplasmic fluorescence following the indicated photobleaching event and the associated quadratic fit. Red triangles denote data points used for steady-state estimates.

(G) Single cell data for cytoplasmic steady-state fluorescence after normalization to its value prior to the first bleaching event for Far1-Venus (red) and YFP (green).

(H) Distribution of coefficients C for the quadratic term of the quadratic fit. C = 0 indicates a linear relationship between the logarithm of the cytoplasmic fluorescence and the number of photobleaching events, which corresponds to the case with no fixed cytoplasmic pool. C > 0 indicates the presence of a fixed cytoplasmic pool (see Supplemental Information).

*denotes $p < 0.05$, ***denotes $p < 0.001$, n.s denotes $p > 0.05$. Tukey boxplots in (D) and (H) indicate median, upper, and lower quartiles. Whiskers extend to the most extreme point within 1.5× the interquartile range.

also tested if the MAPK Fus3 is active in S/G2/M cells (post-*Start*) exposed to pheromone as implied by the above results. Fus3 activity correlates with increased nuclear localization and phosphorylation (Blackwell et al., 2003). We therefore measured Fus3 activity using time lapse microscopy and western blot with a phosphospecific antibody (Nagiec and Dohlman, 2012). Consistent with MAPK (Fus3) activity being responsive to pheromone concentration in cycling cells, Fus3-GFP nuclear localization quickly decreased in cells in the S/G2/M phases of the cell cycle that experienced a drop in extracellular pheromone concentration (Figures S4B–S4D; $p < 10^{-4}$). Similarly, exposure of cells in the S/G2/M phases of the cell cycle to pheromone increased the amount of phosphorylated Fus3 (Figures 3I–3K). Moreover, we immunoprecipitated Fus3 from S/G2/M cells

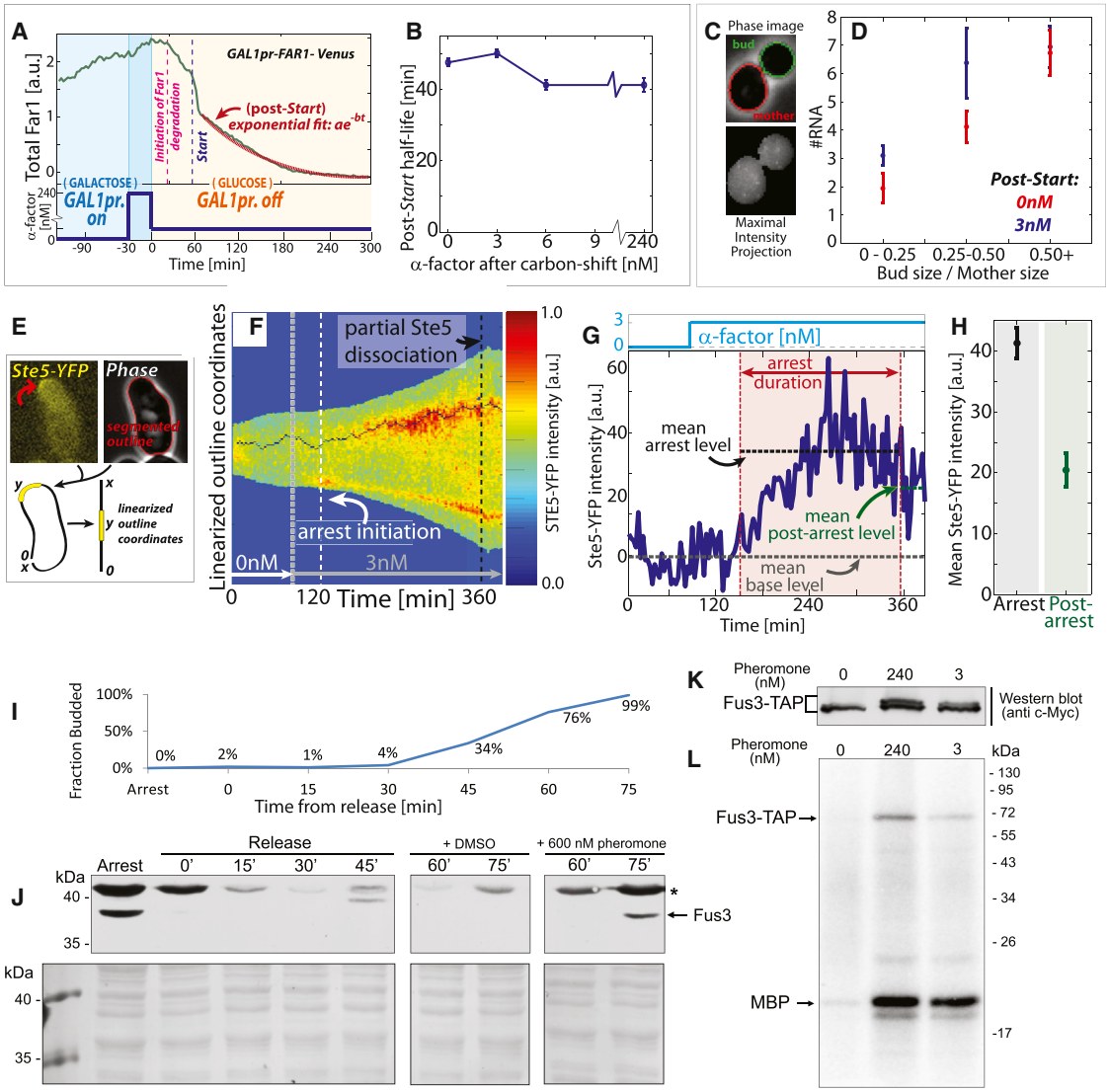

Figure 3. Pheromone Exposure Post-*Start* Is Remembered

(A) Experiment schematic for measuring stability of Far1 protein post-*Start*.

(B) Post-*Start* half-life measured after release from pheromone arrest in 240 nM to 0, 3, 6 and 240 nM.

(C) Example of segmented phase image of mother cell body (red) and bud (green) and their corresponding smFISH maximal intensity projections. Each dot represents a single *FAR1* mRNA.

(D) Mean number of *FAR1* mRNA in cells having small, medium, and large buds.

(E) Example segmented phase and Ste5-YFP fluorescence images for a cell arrested in 3 nM α-factor. Ste5-YFP localizes to the site of polarized growth.

(F) Kymograph of example cell in (E). The amount of Ste5 at the site of polarized growth, whose location was determined using the Viterbi algorithm (Forney, 1973).

(G) Ste5-YFP trace of example cell shown in (F) indicating levels before, after, and during arrest.

(H) Mean Ste5-YFP intensity at the site of polarized growth for pre- and post-*Start* cells in 3 nM. Membrane fluorescence prior to pheromone addition was background subtracted. $p < 0.05$ for all comparisons.

(I–L) Cells were arrested in G1 using pheromone and released synchronously through the cell cycle. Fifty minutes after release, after commitment to division, cells were re-exposed to pheromone (see methods). (I) Bud index. (J) Top: western blot time course with a phospho-specific antibody indicates presence of phosphorylated Fus3 in S/G2/M cells exposed to pheromone; (bottom) Ponceau stained blots are provided as loading controls. (K and L) Fus3-TAP was immunoprecipitated at the 75 min time point, when nearly all cells were in S/G2/M, for cells in 0, 3 or 240 nM pheromone. (K) Western blot for this IP indicating increasing Fus3 phosphoshifts in 3 and 240 nM pheromone. (L) Fus3 activity on MBP was measured in an in vitro kinase assay using radiolabeling.

Error bars in (B), (D) and (H) denote SEM.

exposed to 0, 3 and 240 nM pheromone. IP-Fus3 phosphorylated a substrate (MBP) at a rate increasing with pheromone concentration (Figure 3L).

Taken together, our data support a model in which cells cycling in intermediate pheromone concentrations have increased cytoplasmic Far1 levels due to a partially active

MAPK pathway post-*Start*. Thus, while it is clear that cell-cycle progression inhibits pheromone signaling (Garrenton et al., 2009; Strickfaden et al., 2007; Torres et al., 2011), this inhibition is not complete at intermediate pheromone concentrations. Our data thus shows that intergenerational memory is composed of Far1 accumulated from the entire previous cell division cycle. In other words, cells remember pheromone exposure post-*Start* as well as pre-*Start* from the previous cell division cycle.

Decreasing Cytoplasmic Far1 Reduces Intergenerational Memory

Our results so far support the model in which an *intergenerational* memory of pheromone exposure is transmitted to newborn daughter cells via stable cytoplasmic Far1. If true, we predict that reducing inherited Far1 by genetic manipulation would result in shorter arrest durations in daughter cells. It was previously shown that deletion of the S-phase cyclins *CLB5* and *CLB6,* but not the G1 cyclins *CLN1* and *CLN2*, resulted in longer arrest durations in 3 nM pheromone (Doncic and Skotheim, 2013) and that ectopic expression of Clb5 downregulates Far1 (Oehlen et al., 1998). In addition, the S-phase cyclins are nuclear, where Far1 is rapidly degraded (Blondel et al., 2000; Shirayama et al., 1999). We therefore constructed a *CLB5-NES* strain by adding a nuclear export sequence to *CLB5* (Figure 4A). In this strain, the time to half-maximum post-*Start* of cytoplasmic Far1 in 3 nM pheromone was ~45 min, a significant reduction from the ~75 min half-maximum of wild-type cells (Figures 4B and 4C and S5A,B; $p < 0.01$).

In G1, Far1 will be stable because Clb5 is targeted for degradation by the APC/C following mitosis (Shirayama et al., 1999). Thus, while *CLB5-NES* cells have less cytoplasmic Far1, we expect the smaller amount of inherited Far1 to be just as functional in restraining passage through *Start* as in WT cells. That is, given the same amount of inherited Far1, *CLB5-NES* cells would arrest for similar durations as WT cells. Consistent with these predictions, *CLB5-NES* cells inherited less Far1 and remained arrested for shorter durations relative to WT (Figures 4D, 4E, and S5C). Also as predicted, the relationship between inherited Far1 and arrest duration was statistically similar to WT (Figures 4F and 4G; $p > 0.1$). These data support the interpretation that the *CLB5-NES* allele affects intergenerational memory through a reduction in inherited cytoplasmic Far1 prior to cytokinesis.

Reducing Inherited Far1 Lowers Mating Efficiency

While our results indicate an intergenerational memory of pheromone exposure from mother to daughter cells, it remains unclear if this intergenerational memory plays a role under other physiological conditions. To test this possibility, we performed a quantitative mating assay using WT and *CLB5-NES* strains. WT cells are able to mate more frequently than *CLB5-NES* cells (Figure 4H, $p < 0.05$). To test that this decrease in mating frequency was not due to a polarization defect we verified that *CLB5-NES* cells polarize similarly to WT cells in presence of a pheromone gradient (Figure S5D). These experiments are consistent with a role for intergenerational memory in physiological conditions.

Far1 Binding to Cdc24 Is Required for Intergenerational Memory

Our results so far identify an intergenerational memory arising from the stability of cytoplasmic Far1. This implies that a non-shuttling cytoplasmic pool of Far1 is inherited to transmit intergenerational memory. Consistent with this model, Far1 has binding partners in the cytoplasm, which we hypothesize serve to anchor Far1. A prime candidate for anchoring is Cdc24, a GTP exchange factor (GEF) regulating cell polarization. Far1 binding to Cdc24 is necessary for pheromone gradient sensing, but not for cell-cycle arrest (Nern and Arkowitz, 1999; Valtz et al., 1995) (Figure 5A). Moreover, Cdc24 is nuclear in G1, but is partially exported to the cytoplasm and plasma membrane during mating arrest in a Far1-dependent manner (Nern and Arkowitz, 2000; Shimada et al., 2000).

To test whether the interaction between Cdc24 and Far1 is required for intergenerational memory, we created strains with the endogenous *FAR1* allele replaced by either *FAR1-D1A* or *FAR1-H7* mutant alleles that express Far1 proteins whose interaction with Cdc24 is greatly reduced (Nern and Arkowitz, 2000; Valtz et al., 1995). As previously reported, both strains arrest in pheromone. However, we identified a slight arrest deficiency and 6 nM pheromone was required to arrest cells for similar durations as WT cells in 3 nM ($p > 0.05$). We therefore used 6 nM for the analysis of *FAR1-D1A* and *FAR1-H7* strains. Consistent with Cdc24 anchoring Far1 in the cytoplasm during arrest, the nuclear fraction of Far1 was increased in *FAR1-D1A* and *FAR1-H7* cells compared to WT cells ($p < 10^{-3}$; Figures 5B, S6A, and S6B). Since nuclear Far1 is rapidly degraded in the cell cycle (Figure 1D), we expected that reduction of cytoplasmic anchoring results in a more rapidly degraded Far1 protein. Indeed, Far1 proteins with reduced Cdc24 interactions reach half-maximum concentration more rapidly following cell-cycle entry (Figures 5C, S6C, and S6D). Finally, we examined the relationship between intergenerational memory and inherited Far1 in *FAR1-D1A* and *FAR1-H7* cells. Consistent with the requirement of a cytoplasmic anchor, and the model that Cdc24 fills this role, post-*Start* Far1 was less stable, less Far1 was inherited, and the intergenerational memory was abolished or greatly reduced in cells expressing Far1 proteins with reduced ability to bind Cdc24 (Figures 5D–5F and S6E–S6G).

To further test the Cdc24 anchoring model, we sought to examine *bni1Δ* cells that are unable to export Cdc24 from the nucleus to the shmoo tip during pheromone arrest (Qi and Elion, 2005). Bni1 is a formin that regulates the polarization of actin cables during mating arrest and is required for cell polarization (Evangelista et al., 1997). We found that *bni1Δ* cells arrested as round cells for significant periods of time in G1 when exposed to 6 nM pheromone (Figure S6H). Under these conditions, *bni1Δ* cells contained a higher fraction of nuclear Far1, and degraded Far1 more rapidly upon cell-cycle entry compared to WT cells (Figures 5B, 5C, S6B, and S6C). Finally, *bni1Δ* cells exhibited no intergenerational memory (Figure 5G). That the localization of Cdc24 outside the nucleus was required for intergenerational memory further supports the role of cytoplasmic Cdc24 as a Far1 anchor.

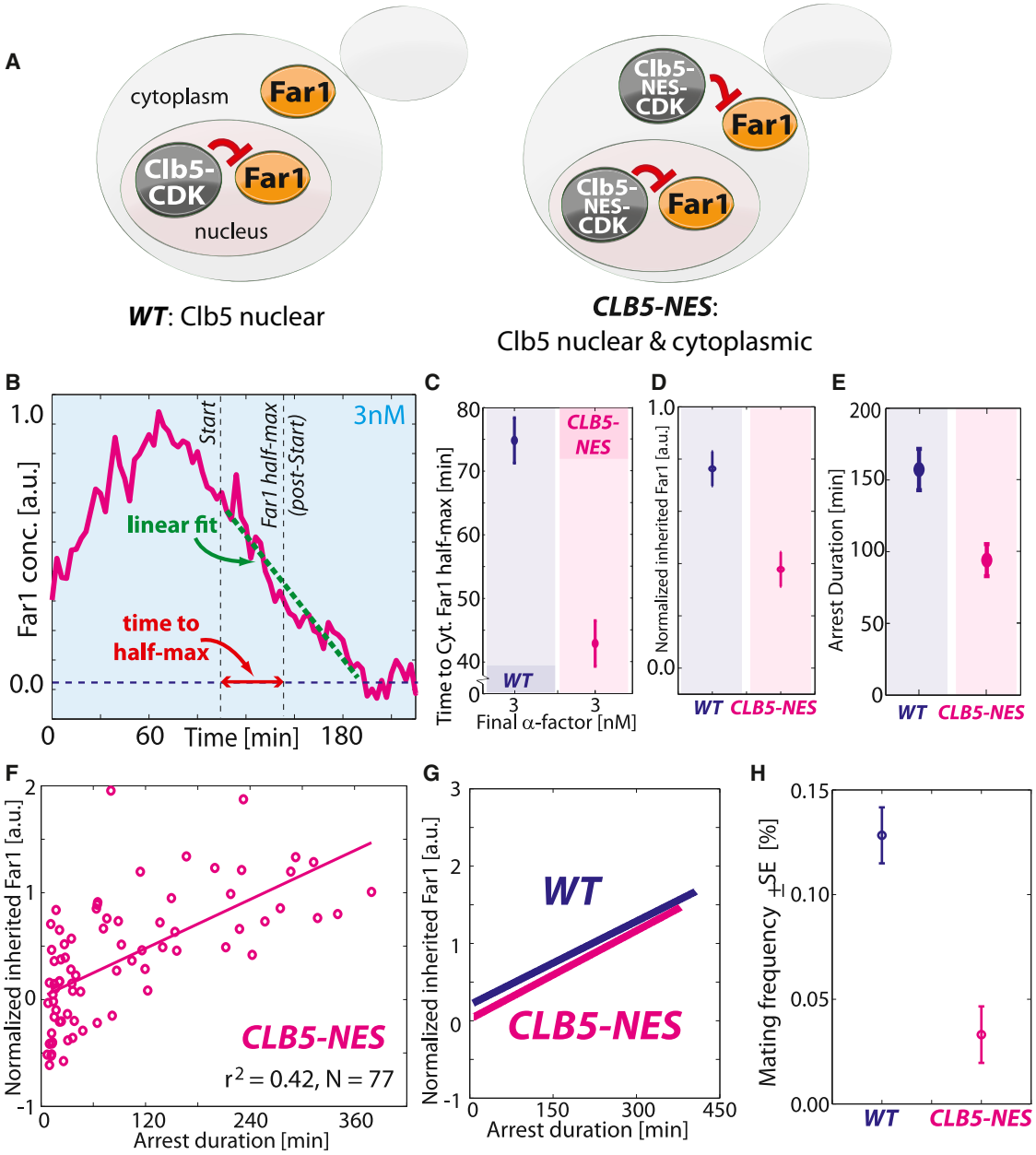

Figure 4. Reduction of Cytoplasmic Far1 Decreases Intergenerational Memory

(A) Clb5 targets Far1 for degradation and is predominantly nuclear in WT cells. Adding a nuclear exclusion sequence (NES) to *CLB5* translocates a fraction to the cytoplasm to target cytoplasmic Far1.

(B) Example time series of Far1 concentration in a *CLB5-NES* cell used to calculate the time to half-maximum post-*Start* for cytoplasmic Far1.

(C) Mean time to cytoplasmic Far1 half-maximum post-*Start* for WT and *CLB5-NES* cells first arrested in 240 nM and then released into 3 nM α-factor.

(D) *CLB5-NES* cells inherit less Far1 than WT and (E) arrest significantly shorter duration ($p < 10^{-5}$).

(F and G) The relationship between the amount of inherited Far1 and the duration of the subsequent arrest is statistically indistinguishable for *CLB5-NES* and WT cells ($p > 0.05$).

(H) WT and *CLB5-NES* cells exhibit significantly different mating frequencies ($p < 0.05$).

Error bars denote SEM of cells in (C–E) or of replica experiments in (H).

Far1 Stability Pre- and Post-*Start* Is Required for Intra- and Inter-Generational Memory Respectively

The intergenerational memory that we describe here is in addition to the *intragenerational memory* of pheromone exposure encoded in Far1 that we previously described (Doncic and Skotheim, 2013). Intragenerational memory allows cells to remember their history of exposure to pheromone during an arrest via the accumulation of Far1. Since Clb5 is targeted for

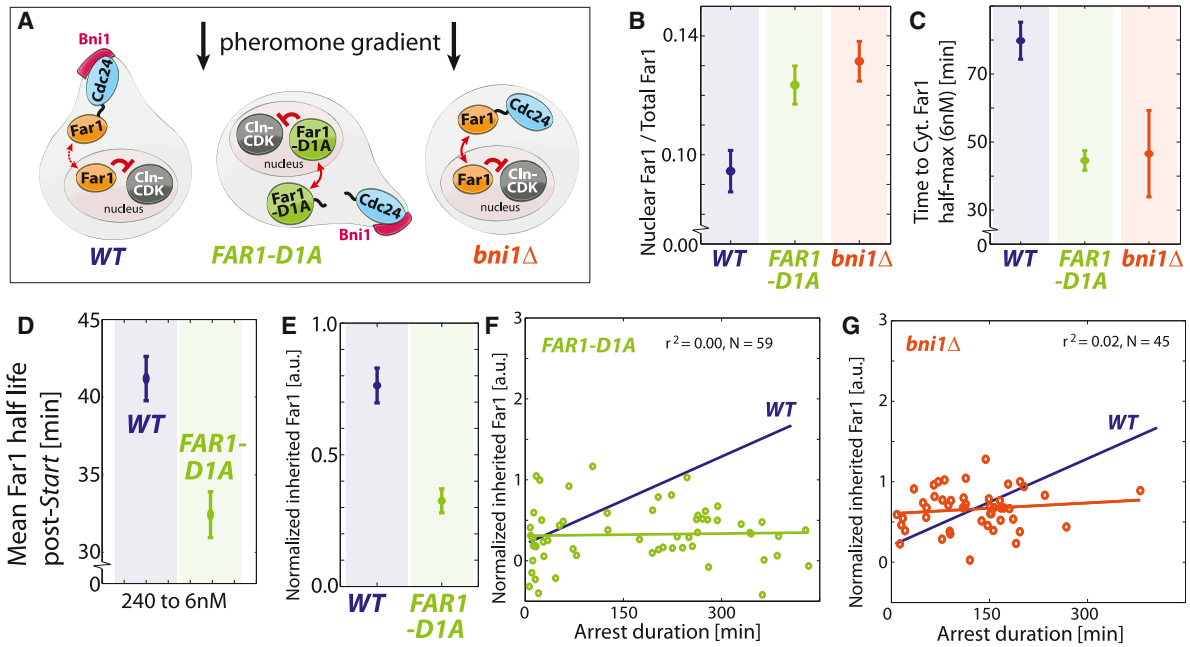

Figure 5. Far1 Binding to Cytoplasmic Cdc24 Is Required for Intergenerational Memory

(A) Schematic of the role of Cdc24 with respect to Far1.

(B) Fraction of nuclear Far1 in arrested cells.

(C) Time to half-maximum Far1 after cell-cycle reentry in 6 nM pheromone.

(D) The post-*Start* stability of Far1-D1A measured as described in Figure 3A.

(E) Inherited Far1 in *FAR1-D1A* cells compared to *WT* ($p < 10^{-4}$).

(F and G) No intergenerational memory was observed for *FAR1-D1A* and *bni1Δ* cells.

Error bars in (B–E) denote SEM.

degradation in mitosis, and is therefore not active during pheromone arrest, we do not expect cytoplasmic Clb5 to affect intragenerational memory. To test this prediction, we examined cell-cycle progression in cells exposed to different histories of mating pheromone during G1. Cells were either exposed to a brief pulse of high pheromone followed by an intermediate pheromone concentration or just to the intermediate pheromone concentration (Figure 6A). As predicted, both WT and *CLB5-NES* cells experiencing the high pheromone pulse greatly extended arrest duration indicating that while *CLB5-NES* cells have reduced intergenerational memory, their intragenerational memory remains firmly intact (Figures 6B and S7A–S7D). Furthermore, these experiments demonstrate how intergenerational memory is distinct from intragenerational memory and affected by different mutations.

Just as intergenerational memory depends on the stability of Far1 throughout the cell cycle, intragenerational memory should depend on the stability of Far1 during arrest. To destabilize Far1 during pheromone arrest, we generated a *FAR1* allele with the 92nd residue mutated from Leucine to Proline (*FAR1-L92P*). This mutation is predicted to generate an additional Cdk consensus phosphorylation site to enhance the degradation of Far1 (E.V. and M.L., unpublished data; Figure S7E). To control for the potentially pleiotropic effects of the L92P mutation, we also generated a *FAR1-PEST* allele, where an otherwise WT *FAR1* allele was fused to the C terminus of *CLN2,* which destabilizes this cyclin (Lanker et al., 1996). To determine the stability of Far1-L92P and Far1-PEST proteins during arrest, we fused them to GFP and expressed them from a *GAL1* promoter. Consistent with these mutations reducing protein stability, the pre-*Start* half-lives of Far1-L92P and Far1-PEST were reduced to ~50 and ~20 min respectively compared to over 130 min for WT Far1 (Figures 6C and 6D).

To test the dependence of intragenerational memory on Far1 stability, we next constructed a strain containing a single copy of *FAR1-L92P* expressed from its endogenous locus. However, *FAR1-L92P* cells failed to arrest even at high pheromone concentrations. We therefore constructed a strain containing 10-12 copies of *FAR1-L92P* that arrested as WT cells (72 ± 4 min for WT and 61 ± 7 min for *FAR1-L92P* in 2.7 nM pheromone, p = 0.17). To verify that the activity of Far1 remains unaltered in the *FAR1-L92P* strain we also showed that the ability of *12xFAR1-L92P* cells to polarize toward pheromone gradients was similar to WT cells (Figure S7F). Consistent with memory depending on Far1 stability, *12xFAR1-L92P* cells exhibited little if any intragenerational memory despite retaining the ability to arrest at this pheromone concentration (Figures 6B and S7A–S7C). In addition, *12xFAR1-L92P* cells also exhibit no intergenerational memory, most likely because this phenomenon also depends on Far1 stability (Figure 6E). Similarly, the destabilized *FAR1-PEST* strain greatly reduced both intra- and inter-generational memory (Figures 6B, 6F, S7A, and S7G). Taken together, these experiments

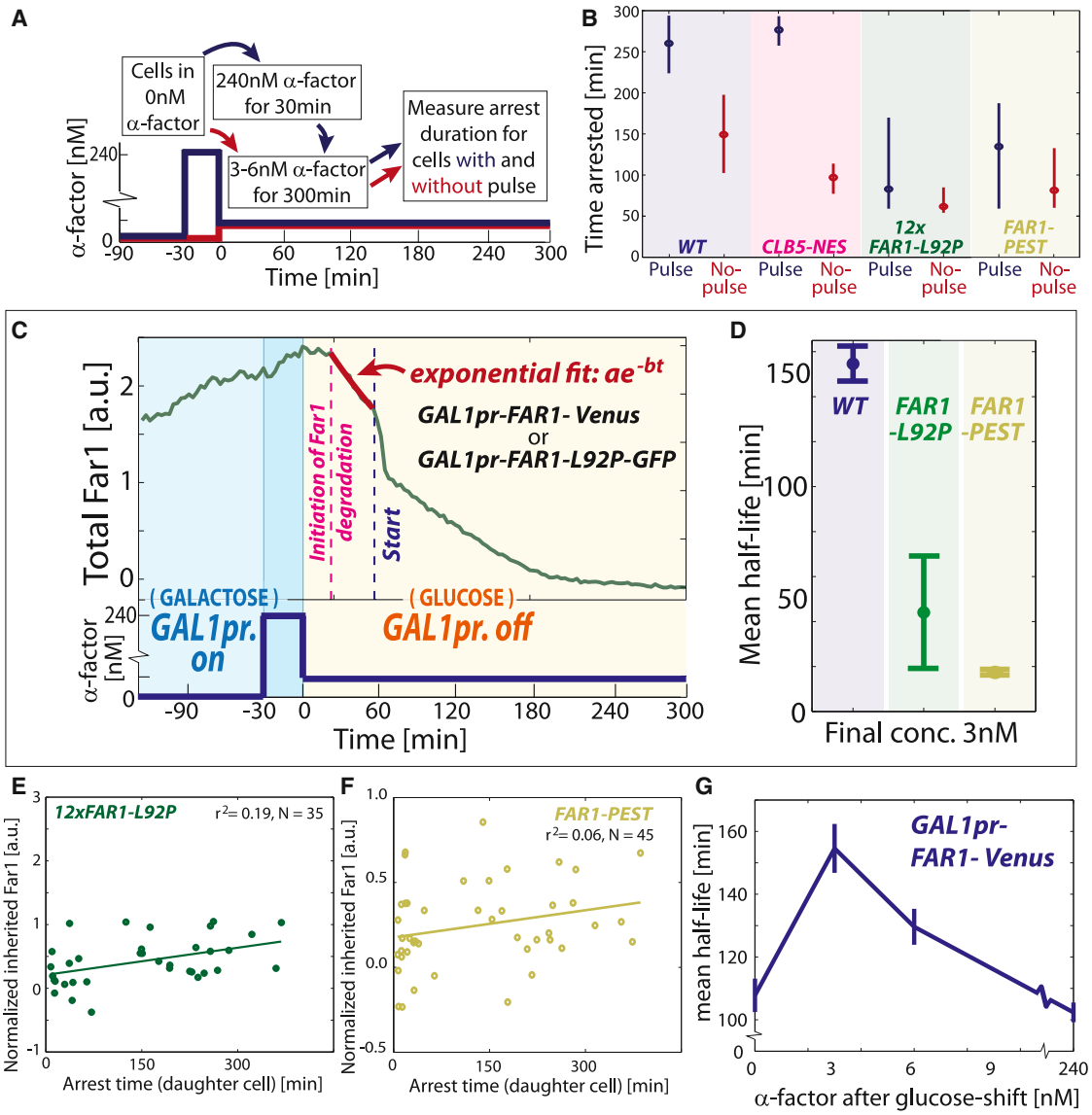

Figure 6. Protein Stability Is Required for Intra- and Inter-Generational Memory

(A) Experimental schematic for *intragenerational* memory experiment.

(B) WT and *CLB5-NES* cells have intragenerational memory, where the decision to reenter the cell cycle is based on the history of pheromone exposure during the arrest, while *12xFAR1-L92P* and *FAR1-PEST* cells do not. Medians plotted with 95% confidence intervals computed using 10,000 bootstrap iterations. Note that about half of both the *CLB5-NES* and WT cells exposed to a pulse of high mating pheromone are arrested for the duration of the experiment (Figure S7B). We therefore do not compare arrest durations for WT and *CLB5-NES* cells exposed to a pheromone pulse.

(C) Conditional expression of *FAR1* from a *GAL1* promoter is used to measure half-life pre-*Start* in a series of pheromone concentrations.

(D) Far1 half-life pre-*Start* in WT, *FAR1-L92P*, and *FAR1-PEST* cells in 3 nM α-factor.

(E and F) *12xFAR1-L92P* and *FAR1-PEST* cells lack intergenerational memory as their arrest duration is independent of the amount of inherited Far1.

(G) Conditional expression from a *GAL1* promoter is used to measure Far1 half-life ± SE pre-*Start* as in (C), but for a range of pheromone concentrations. Error bars in (D) and (G) denote SEM.

demonstrate the requirement of Far1 stability pre- and post-*Start* for intra- and inter-generational memory respectively.

Far1 Stability during Arrest Peaks at Intermediate Pheromone Concentrations

The clear connection between Far1-based memory and protein stability suggested the possibility that WT cells might modulate Far1 stability to regulate memory. To test this possibility, we measured *FAR1* half-life by expressing it from the *GAL1* promoter and shutting off transcription (Figure 6C). However, we now measure the half-life during pre-*Start* for cells growing in 0, 3, 6, or 240 nM pheromone. We found that Far1 stability peaked at 3 nM with a ~150 min half-life (Figures 6G and S7H and S7I). Far1 stability was reduced to ~100 min in

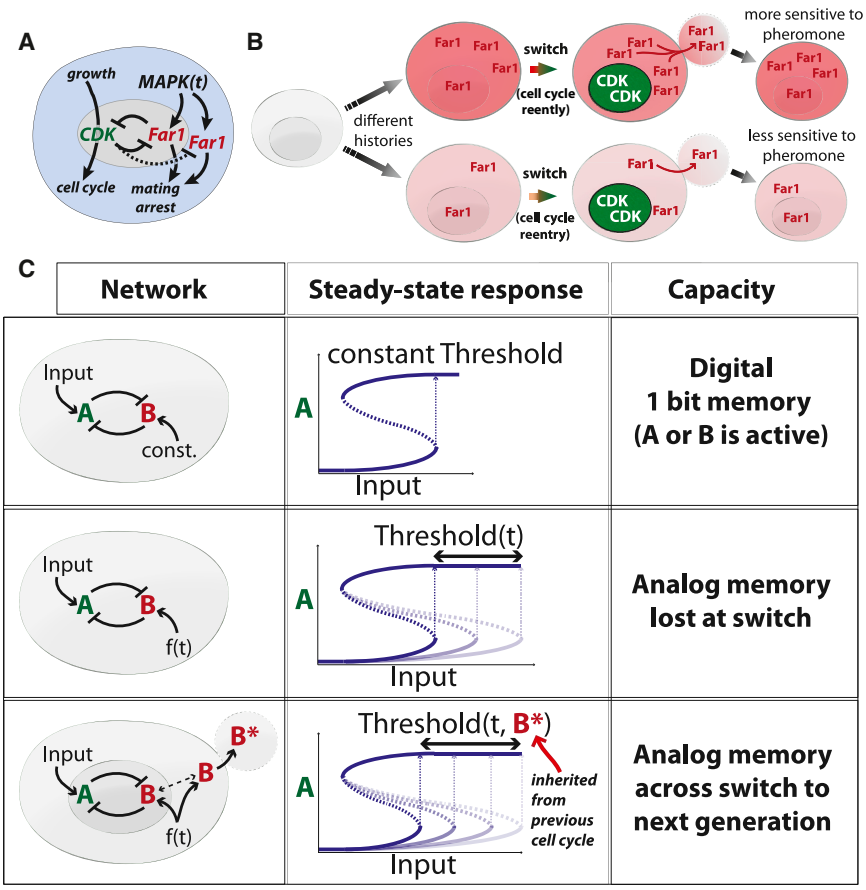

Figure 7. Compartmentalization Enables Analog Memory to Pass through a Bistable Switch

(A) The *Start* regulatory network regulating the proliferation-differentiation decision in budding yeast is a bistable switch.

(B) Inheritance of cytoplasmic Far1 forms the mechanistic basis of intergenerational memory of pheromone exposure.

(C) Top: a double-negative switch with constant signal activating B results in a bistable switch with a single bit of memory, i.e., did the input approach its current level from above or below. Middle: a time-dependent f(t) signal activates B to allow the time-dependent threshold to encode an analog memory of f(t). However, this memory is lost by inactivation upon triggering the double-negative switch. Bottom: compartmentalization allows transmission of analog memory of the time-dependent f(t) signal across the double-negative (positive) feedback switch.

0 and 240 nM pheromone. We speculate that this decreased stability might arise from increased G1 cyclin and Fus3 MAPK kinase activities. It is interesting to note that the maximum half-life, i.e., maximal memory, occurs right where the decision to reenter the cell cycle is most sensitive to pheromone concentration.

DISCUSSION

To inform our decisions, our experiences are sensed, encoded, and stored as memories. Like us, individual cells also rely on past experience to inform their most important decisions. In budding yeast, one of the most important decisions is whether or not to proliferate or to arrest division and attempt to mate with another haploid cell. Budding yeast invest heavily in this decision, as mutations eliminating the ability to mate provide a ~2% growth rate advantage in pheromone-free conditions (Lang et al., 2009). Perhaps not surprisingly, several distinct types of memory regulate this proliferation-differentiation decision.

The simplest type of memory informing yeast mating is binary and stored as a single bit of information. For example, due to its asymmetric division pattern, a budding yeast cell is either a mother or a daughter. With regards to mating, this bit matters because mother cells are less sensitive to pheromone than daughter cells (Moore, 1984). In part, this is likely due to the differential expression of *CLN3,* the upstream cyclin driving cell-cycle progression in G1 (Laabs et al., 2003). Mother cells produce a burst of *CLN3* expression at the transition from mitosis to G1, while daughter cells do not due to the daughter-specific transcription factors, Ace2 and Ash1 (Di Talia et al., 2009). In addition, differential post-transcriptional regulation of *CLN3* in mother and daughter cells may be due to Whi3 (Caudron and Barral, 2013), which both decreases *CLN3* message stability and translation rate (Cai and Futcher, 2013; Garí et al., 2001; Holmes et al., 2013). Yet, all this information pertaining being a mother or daughter cell is binary.

Previously, we identified a continuous, analog form of memory of past pheromone exposure that informs the decision to reenter the cell cycle from pheromone arrest (Doncic and Skotheim, 2013). Cells experiencing higher pheromone concentrations over longer periods of time are more reluctant to reenter the cell cycle. While MAPK pathway activity rapidly responds to reflect the current extracellular pheromone concentration, proteins are more stable so that their level will reflect an integral of past pathway activity (Colman-Lerner et al., 2005; Takahashi and Pryciak, 2008; Yu et al., 2008). More specifically, Far1 accumulates at a monotonically increasing rate with pheromone concentration so that its total amount reflects a combination of arrest duration and pheromone concentration (Chang and Herskowitz, 1990; Doncic and Skotheim, 2013). Thus, the amount of Far1 accumulated during pheromone arrest reflects an integral of pathway activity over time that encodes the history of pheromone exposure into a continuous analog rather than binary variable. However, the mutual inhibition of Far1 and Cdk activities suggested that this analog memory, i.e., the accumulated Far1, would be lost upon flipping the cell-cycle switch (Figures 7A–7C).

Here, we show how the distribution of Far1 into nuclear and cytoplasmic compartments is used to transmit the analog memory of pheromone exposure across the cell cycle switch to the next generation. While nuclear Far1 is rapidly degraded, as expected by the double-negative switch, cytoplasmic Far1 is longer lived and continually synthesized so that a significant amount remains at the end of the cell cycle to be inherited by daughter cells. We show here that this inherited Far1 contributes to increased pheromone sensitivity and thereby allows mother cells to transmit intergenerational memory of pheromone exposure to their daughter cells. We also identified a fraction of fixed cytoplasmic Far1 as key to storing intergenerational memory. If some Far1 were not fixed in the cytoplasm, it would likely be rapidly degraded post-*Start* due to the high nuclear B-type cyclin activity. While this Far1 fraction is fixed on the minute timescale, we suspect that it is not permanently fixed because nuclear Far1 is important for maintaining the cell-cycle arrest to which the inherited cytoplasmic Far1 eventually contributes. Thus, the slow dissociation of the fixed Far1 is likely central to reading the intergenerational memory of pheromone exposure.

Protein stability is central to both intra- and intergenerational Far1-based analog memory as destabilizing mutations eliminate both. In general, protein stability determines the timescale on which the cell can remember past events. For rapidly degraded proteins, levels will simply reflect the current state of the cell, while for stable proteins, levels will reflect their synthesis over longer periods of time so that their amount can be used to store long-term memories on the timescale of dilution due to cell growth. The demonstrated ability of the cell to regulate protein stability over a wide range of temporal and spatial scales suggests that the analog memory mechanisms discussed here can be easily tuned through mutation and selection.

More broadly, our work illustrates how spatial organization can greatly expand the functionality of signaling motifs. Recently, it has been shown how positive feedback can be enhanced by protein transport within the mammalian mitotic switch (Santos et al., 2012). Activation of Cdk1-Cyclin B complexes within the nucleus recruit additional such complexes to dramatically ramp up nuclear Cdk activity without protein synthesis. However, this represents an enhancement of the well-known ability of positive feedback circuits to generate sharp switches. Here, we have shown how spatial organization allows memory to be transmitted across a positive feedback-driven switch to enable an entirely new and unexpected property of this well-characterized signaling motif. Given the extensive spatial organization within cells, we expect this example to be the first of many in which new signal-processing properties of network motifs are enabled by compartmentalization.

EXPERIMENTAL PROCEDURES

See additional Supplemental Information for methods regarding confocal microscopy, FRAP, western blot and kinase assays shown in Figures 2 and 3.

Wide-Field Time Lapse Microscopy and Analysis

A Zeiss Observer Z1 microscope with an automated stage using a plan-apo 63X/1.4NA oil immersion objective and Definite Focus hardware was used to take images every 3 min (6 min for the *FAR1-L92P* strains). We used a Cellasic microfluidics device (http://www.cellasic.com/) with Y04C plates. *WHI5-mCherry, FAR1-Venus* and *FAR1-GFP* strains were exposed for 750 ms, 300 ms or 150–300 ms using the Colibri 540-80, 505 or 470 LED modules respectively at 25% power. There was no significant photobleaching at our sampling rate (Figure S7J). *FAR1* activity is not affected by fusion to a fluorescent protein (Doncic and Skotheim, 2013). Image segmentation and quantification was performed as described in (Doncic et al., 2013). We often plot mean values and their associated SE because this gives a graphical representation of statistical significance. Corresponding full distributions can be found in the Supplemental Information.

Measurement of Inherited Far1

For each cell we determine inherited Far1 to be (Far1-Venus signal – baseline)/(baseline). "Normalized inherited Far1" is the amount at the beginning of G1 above what that cell would be expected to have when cycling in pheromone-free media (see also schematic S2I and Supplemental Information for details).

Strains and Media

All strains are congenic with W303 (see Table S1) and were constructed using standard methods. Yeast were grown in synthetic complete media with 2% glucose unless otherwise stated (2% galactose were used for the Far1 stability experiments in Figures 3 and 6). Before an experiment, cells were grown to an OD < 0.1 after which they were sonicated for ~5 s at 3W intensity. All media were mixed with 20 mg/ml casein (Sigma) to inhibit α-factor surface adhesion (Colman-Lerner et al., 2005).

SUPPLEMENTAL INFORMATION

Supplemental Information includes Extended Experimental Procedures, seven figures, and two tables and can be found with this article online at http://dx.doi.org/10.1016/j.cell.2015.02.032.

AUTHOR CONTRIBUTIONS

A.D. and J.M.S. designed the study. A.D. and O.A. performed all experiments with the following exceptions. E.V. and M.L. identified of the *FAR1-L92P* mutant and performed the Fus3 activity measurements (Figures 3I–3L). A.G., A.B., G.V., and A.C.-L. performed the FRAP experiments (Figure 2). A.D., O.A., and J.M.S. wrote the paper.

ACKNOWLEDGMENTS

Research in the Skotheim laboratory was supported by the Burroughs Wellcome Fund (CASI) and the NIH (GM092925). The Colman-Lerner laboratory was supported by grant PICT2010-2248 from the Argentine Agency of Research and Technology (ANPCyT) and the NIH (GM097479), while the Loog laboratory was supported by Estonian Science Agency Grant IUT2-21.

Received: July 27, 2014
Revised: November 24, 2014
Accepted: January 17, 2015
Published: March 12, 2015

REFERENCES

Alon, U. (2007). Network motifs: theory and experimental approaches. Nat. Rev. Genet. *8*, 450–461.

Behar, M., Hao, N., Dohlman, H.G., and Elston, T.C. (2008). Dose-to-duration encoding and signaling beyond saturation in intracellular signaling networks. PLoS Comput. Biol. *4*, e1000197.

Blackwell, E., Halatek, I.M., Kim, H.J., Ellicott, A.T., Obukhov, A.A., and Stone, D.E. (2003). Effect of the pheromone-responsive G(alpha) and phosphatase proteins of Saccharomyces cerevisiae on the subcellular localization of the Fus3 mitogen-activated protein kinase. Mol. Cell. Biol. *23*, 1135–1150.

Blondel, M., Alepuz, P.M., Huang, L.S., Shaham, S., Ammerer, G., and Peter, M. (1999). Nuclear export of Far1p in response to pheromones requires the export receptor Msn5p/Ste21p. Genes Dev. *13*, 2284–2300.

Blondel, M., Galan, J.M., Chi, Y., Lafourcade, C., Longaretti, C., Deshaies, R.J., and Peter, M. (2000). Nuclear-specific degradation of Far1 is controlled by the localization of the F-box protein Cdc4. EMBO J. *19*, 6085–6097.

Cai, Y., and Futcher, B. (2013). Effects of the yeast RNA-binding protein Whi3 on the half-life and abundance of CLN3 mRNA and other targets. PLoS ONE *8*, e84630.

Caudron, F., and Barral, Y. (2013). A super-assembly of Whi3 encodes memory of deceptive encounters by single cells during yeast courtship. Cell *155*, 1244–1257.

Chang, F., and Herskowitz, I. (1990). Identification of a gene necessary for cell cycle arrest by a negative growth factor of yeast: FAR1 is an inhibitor of a G1 cyclin, CLN2. Cell *63*, 999–1011.

Chen, R.E., and Thorner, J. (2007). Function and regulation in MAPK signaling pathways: lessons learned from the yeast Saccharomyces cerevisiae. Biochim. Biophys. Acta *1773*, 1311–1340.

Colman-Lerner, A., Gordon, A., Serra, E., Chin, T., Resnekov, O., Endy, D., Pesce, C.G., and Brent, R. (2005). Regulated cell-to-cell variation in a cell-fate decision system. Nature *437*, 699–706.

Costanzo, M., Nishikawa, J.L., Tang, X., Millman, J.S., Schub, O., Breitkreuz, K., Dewar, D., Rupes, I., Andrews, B., and Tyers, M. (2004). CDK activity antagonizes Whi5, an inhibitor of G1/S transcription in yeast. Cell *117*, 899–913.

de Bruin, R.A., McDonald, W.H., Kalashnikova, T.I., Yates, J., 3rd, and Wittenberg, C. (2004). Cln3 activates G1-specific transcription via phosphorylation of the SBF bound repressor Whi5. Cell *117*, 887–898.

Di Talia, S., Wang, H., Skotheim, J.M., Rosebrock, A.P., Futcher, B., and Cross, F.R. (2009). Daughter-specific transcription factors regulate cell size control in budding yeast. PLoS Biol. *7*, e1000221.

Doncic, A., and Skotheim, J.M. (2013). Feedforward regulation ensures stability and rapid reversibility of a cellular state. Mol. Cell *50*, 856–868.

Doncic, A., Falleur-Fettig, M., and Skotheim, J.M. (2011). Distinct interactions select and maintain a specific cell fate. Mol. Cell *43*, 528–539.

Doncic, A., Eser, U., Atay, O., and Skotheim, J.M. (2013). An algorithm to automate yeast segmentation and tracking. PLoS ONE *8*, e57970.

Errede, B., and Ammerer, G. (1989). STE12, a protein involved in cell-type-specific transcription and signal transduction in yeast, is part of protein-DNA complexes. Genes Dev. *3*, 1349–1361.

Evangelista, M., Blundell, K., Longtine, M.S., Chow, C.J., Adames, N., Pringle, J.R., Peter, M., and Boone, C. (1997). Bni1p, a yeast formin linking cdc42p and the actin cytoskeleton during polarized morphogenesis. Science *276*, 118–122.

Forney, G.D. (1973). Viterbi Algorithm. IEEE *61*, 268–278.

Garí, E., Volpe, T., Wang, H., Gallego, C., Futcher, B., and Aldea, M. (2001). Whi3 binds the mRNA of the G1 cyclin CLN3 to modulate cell fate in budding yeast. Genes Dev. *15*, 2803–2808.

Garrenton, L.S., Braunwarth, A., Irniger, S., Hurt, E., Künzler, M., and Thorner, J. (2009). Nucleus-specific and cell cycle-regulated degradation of mitogen-activated protein kinase scaffold protein Ste5 contributes to the control of signaling competence. Mol. Cell. Biol. *29*, 582–601.

Gartner, A., Jovanović, A., Jeoung, D.I., Bourlat, S., Cross, F.R., and Ammerer, G. (1998). Pheromone-dependent G1 cell cycle arrest requires Far1 phosphorylation, but may not involve inhibition of Cdc28-Cln2 kinase, in vivo. Mol. Cell. Biol. *18*, 3681–3691.

Hao, N., Nayak, S., Behar, M., Shanks, R.H., Nagiec, M.J., Errede, B., Hasty, J., Elston, T.C., and Dohlman, H.G. (2008). Regulation of cell signaling dynamics by the protein kinase-scaffold Ste5. Mol. Cell *30*, 649–656.

Hartwell, L.H., Culotti, J., Pringle, J.R., and Reid, B.J. (1974). Genetic control of the cell division cycle in yeast. Science *183*, 46–51.

Henchoz, S., Chi, Y., Catarin, B., Herskowitz, I., Deshaies, R.J., and Peter, M. (1997). Phosphorylation- and ubiquitin-dependent degradation of the cyclin-dependent kinase inhibitor Far1p in budding yeast. Genes Dev. *11*, 3046–3060.

Holmes, K.J., Klass, D.M., Guiney, E.L., and Cyert, M.S. (2013). Whi3, an S. cerevisiae RNA-binding protein, is a component of stress granules that regulates levels of its target mRNAs. PLoS ONE *8*, e84060.

Howell, A.S., Jin, M., Wu, C.F., Zyla, T.R., Elston, T.C., and Lew, D.J. (2012). Negative feedback enhances robustness in the yeast polarity establishment circuit. Cell *149*, 322–333.

Jeoung, D.I., Oehlen, L.J., and Cross, F.R. (1998). Cln3-associated kinase activity in Saccharomyces cerevisiae is regulated by the mating factor pathway. Mol. Cell. Biol. *18*, 433–441.

Kholodenko, B.N., Hancock, J.F., and Kolch, W. (2010). Signalling ballet in space and time. Nat. Rev. Mol. Cell Biol. *11*, 414–426.

Laabs, T.L., Markwardt, D.D., Slattery, M.G., Newcomb, L.L., Stillman, D.J., and Heideman, W. (2003). ACE2 is required for daughter cell-specific G1 delay in Saccharomyces cerevisiae. Proc. Natl. Acad. Sci. USA *100*, 10275–10280.

Lang, G.I., Murray, A.W., and Botstein, D. (2009). The cost of gene expression underlies a fitness trade-off in yeast. Proc. Natl. Acad. Sci. USA *106*, 5755–5760.

Lanker, S., Valdivieso, M.H., and Wittenberg, C. (1996). Rapid degradation of the G1 cyclin Cln2 induced by CDK-dependent phosphorylation. Science *271*, 1597–1601.

Lee, M.J., Ye, A.S., Gardino, A.K., Heijink, A.M., Sorger, P.K., MacBeath, G., and Yaffe, M.B. (2012). Sequential application of anticancer drugs enhances cell death by rewiring apoptotic signaling networks. Cell *149*, 780–794.

Malleshaiah, M.K., Shahrezaei, V., Swain, P.S., and Michnick, S.W. (2010). The scaffold protein Ste5 directly controls a switch-like mating decision in yeast. Nature *465*, 101–105.

McKinney, J.D., Chang, F., Heintz, N., and Cross, F.R. (1993). Negative regulation of FAR1 at the Start of the yeast cell cycle. Genes Dev. *7*, 833–843.

Moore, S.A. (1984). Yeast cells recover from mating pheromone alpha factor-induced division arrest by desensitization in the absence of alpha factor destruction. J. Biol. Chem. *259*, 1004–1010.

Nagiec, M.J., and Dohlman, H.G. (2012). Checkpoints in a yeast differentiation pathway coordinate signaling during hyperosmotic stress. PLoS Genet. *8*, e1002437.

Nern, A., and Arkowitz, R.A. (1999). A Cdc24p-Far1p-Gbetagamma protein complex required for yeast orientation during mating. J. Cell Biol. *144*, 1187–1202.

Nern, A., and Arkowitz, R.A. (2000). Nucleocytoplasmic shuttling of the Cdc42p exchange factor Cdc24p. J. Cell Biol. *148*, 1115–1122.

Oehlen, L.J., McKinney, J.D., and Cross, F.R. (1996). Ste12 and Mcm1 regulate cell cycle-dependent transcription of FAR1. Mol. Cell. Biol. *16*, 2830–2837.

Oehlen, L.J., Jeoung, D.I., and Cross, F.R. (1998). Cyclin-specific START events and the G1-phase specificity of arrest by mating factor in budding yeast. Mol. Gen. Genet. *258*, 183–198.

Peter, M., and Herskowitz, I. (1994). Direct inhibition of the yeast cyclin-dependent kinase Cdc28-Cln by Far1. Science *265*, 1228–1231.

Peter, M., Gartner, A., Horecka, J., Ammerer, G., and Herskowitz, I. (1993). FAR1 links the signal transduction pathway to the cell cycle machinery in yeast. Cell *73*, 747–760.

Pope, P.A., Bhaduri, S., and Pryciak, P.M. (2014). Regulation of Cyclin-Substrate Docking by a G1 Arrest Signaling Pathway and the Cdk Inhibitor Far1. Curr. Biol.

Pryciak, P.M., and Huntress, F.A. (1998). Membrane recruitment of the kinase cascade scaffold protein Ste5 by the Gbetagamma complex underlies activation of the yeast pheromone response pathway. Genes Dev. *12*, 2684–2697.

Purvis, J.E., Karhohs, K.W., Mock, C., Batchelor, E., Loewer, A., and Lahav, G. (2012). p53 dynamics control cell fate. Science *336*, 1440–1444.

Qi, M., and Elion, E.A. (2005). Formin-induced actin cables are required for polarized recruitment of the Ste5 scaffold and high level activation of MAPK Fus3. J. Cell Sci. *118*, 2837–2848.

Raj, A., van den Bogaard, P., Rifkin, S.A., van Oudenaarden, A., and Tyagi, S. (2008). Imaging individual mRNA molecules using multiple singly labeled probes. Nat. Methods *5*, 877–879.

Santos, S.D., Wollman, R., Meyer, T., and Ferrell, J.E., Jr. (2012). Spatial positive feedback at the onset of mitosis. Cell *149*, 1500–1513.

Shimada, Y., Gulli, M.P., and Peter, M. (2000). Nuclear sequestration of the exchange factor Cdc24 by Far1 regulates cell polarity during yeast mating. Nat. Cell Biol. *2*, 117–124.

Shirayama, M., Tóth, A., Gálová, M., and Nasmyth, K. (1999). APC(Cdc20) promotes exit from mitosis by destroying the anaphase inhibitor Pds1 and cyclin Clb5. Nature *402*, 203–207.

Skotheim, J.M., Di Talia, S., Siggia, E.D., and Cross, F.R. (2008). Positive feedback of G1 cyclins ensures coherent cell cycle entry. Nature *454*, 291–296.

Strickfaden, S.C., Winters, M.J., Ben-Ari, G., Lamson, R.E., Tyers, M., and Pryciak, P.M. (2007). A mechanism for cell-cycle regulation of MAP kinase signaling in a yeast differentiation pathway. Cell *128*, 519–531.

Takahashi, S., and Pryciak, P.M. (2008). Membrane localization of scaffold proteins promotes graded signaling in the yeast MAP kinase cascade. Curr. Biol. *18*, 1184–1191.

Thomson, T.M., Benjamin, K.R., Bush, A., Love, T., Pincus, D., Resnekov, O., Yu, R.C., Gordon, A., Colman-Lerner, A., Endy, D., and Brent, R. (2011). Scaffold number in yeast signaling system sets tradeoff between system output and dynamic range. Proc. Natl. Acad. Sci. USA *108*, 20265–20270.

Torres, M.P., Clement, S.T., Cappell, S.D., and Dohlman, H.G. (2011). Cell cycle-dependent phosphorylation and ubiquitination of a G protein alpha subunit. J. Biol. Chem. *286*, 20208–20216.

Tyers, M., and Futcher, B. (1993). Far1 and Fus3 link the mating pheromone signal transduction pathway to three G1-phase Cdc28 kinase complexes. Mol. Cell. Biol. *13*, 5659–5669.

Valtz, N., Peter, M., and Herskowitz, I. (1995). FAR1 is required for oriented polarization of yeast cells in response to mating pheromones. J. Cell Biol. *131*, 863–873.

Yang, Q., and Ferrell, J.E., Jr. (2013). The Cdk1-APC/C cell cycle oscillator circuit functions as a time-delayed, ultrasensitive switch. Nat. Cell Biol. *15*, 519–525.

Yosef, N., and Regev, A. (2011). Impulse control: temporal dynamics in gene transcription. Cell *144*, 886–896.

Yu, R.C., Pesce, C.G., Colman-Lerner, A., Lok, L., Pincus, D., Serra, E., Holl, M., Benjamin, K., Gordon, A., and Brent, R. (2008). Negative feedback that improves information transmission in yeast signalling. Nature *456*, 755–761.

EXTENDED EXPERIMENTAL PROCEDURES

Measurement of Inherited Far1

We measure inherited Far1 in the following way (see schematic S2I). First, we measure the concentration of Far1 in the daughter cell at birth, which we take to be when Far1 is first visible in the nucleus just after mitosis. Since there is substantial variability in fluorescence intensity from experiment-to-experiment and position in the microfluidic chamber, we normalize the daughter Far1 concentration at birth by the baseline concentration of Far1-Venus (or GFP) in the corresponding mother cell in the preceding cell cycle(s). We take inherited Far1 to be the (Far1-Venus signal – baseline)/(baseline). Thus, what we term "normalized inherited Far1" is the amount at the beginning of G1 above and beyond what it would normally have when cycling in pheromone-free media. For some cells in our analysis, only a short part of their preceding cell cycle was in media containing pheromone and so the additional Far1 due to pheromone exposure in the previous cell cycle is small. In this case, negative values can arise if the Far1 level is less than the level in the previous cell cycle. These negative values are not due to Venus signals below the autofluorescence background (see signal-to-noise analysis in the supplementary methods).

Confocal Imaging

YAG5040 cells (*GAL1pr-FAR1-Venus*, *WHI5-mKO*) were grown over night on a Gal-Raf plate before being placed in pheromone-free or high pheromone liquid culture. Cells were imaged using an Olympus FV1000 confocal microscope. Pre-*Start* cells were identified and the nuclear photobleaching area was manually defined using one image from the mKO channel (543 nm laser; 80% power). 128x128 pixel images were acquired at a rate of 0.25px/μs using a 16x zoom and 515 nm laser at 1% power. See supplementary information for a description of the model fit. Data were background subtracted and corrected for photobleaching. The time constant for photobleaching Venus, i.e., the time to bleach 1/e of the initial signal, was ~160 s so that only a very slight correction was required on the timescale of the data presented in Figure 2.

smFISH mRNA Imaging

Single-molecule FISH of *FAR1* mRNA was performed as described in (Raj et al., 2008), and mRNA numbers were determined from a maximal intensity projection of 13 z-stacks of 0.5 μm.

Mating Assay

To measure mating efficiency we used two mating strains (WT and *CLB5-NES*) and one tester strain with complementary amino acid deficiencies so that neither mating nor tester strains could live on plates lacking histidine, adenine, tryptophan, uracil, and leucine. Cells were grown overnight to an OD less than 0.3 and concentrated to OD 2.0. Mating and tester strains were serially diluted and plated on YPD plates to determine the relationship between OD and number of cells. Next, 40 μl of tester strain followed by 10 μl mating strain (at OD 2.0) were pipetted on a 20 μm cellulose membrane on a YPD plate and left for 6 hr to mate at 30°C. After this, cells were washed from the membranes and plated in different dilutions on plates lacking histidine, adenine, tryptophan, uracil, and leucine. Next, the number of colonies was counted and divided by the total number of cells plated to determine mating frequencies.

Stability and Half-Maximum Measurements

To determine the time for cytoplasmic Far1 to reach its half-maximum value, cells were segmented and the base level of Far1 concentration was determined. A linear fit was applied to the Far1 concentration to estimate the time to reach half-maximum. Far1 stability was measured using *GAL1pr-FAR1-Venus* or *GAL1pr-FAR1-GFP* strain as described in Figures 3A and 6C.

Measurements of Fus3 Activity in S/G2/M

For the western blot analysis of phosphorylated Fus3, cells were first grown in YPD media until OD600 = 0.3, then treated for 2.5h with 600 nM pheromone and subsequently released into fresh media by washing with YPD media without the pheromone. After 50 min, DMSO, 3, 240 or 600 nM pheromone was added. Cell extracts were produced by bead-beating in urea lysis buffer and protein concentration was determined by Bio-Rad Protein Assay. Proteins were resolved by 10% SDS-PAGE and blotted with semidry blotter (Bio-Rad). Phosphorylated (activated) Fus3 was detected by immunoblotting with Phospho-p44/42 MAPK antibody (Nagiec and Dohlman, 2012) (#9101, Cell Signaling Technology). For Fus3 immunoprecipitation, cell extracts were produced by bead-beating in TAP lysis buffer (25 mM HEPES [pH 8.0], 500 mM NaCl, 1 mM EDTA, 30 mM EGTA, complete protease and phosphatase inhibitor cocktail). To immunoprecipitate Fus3, clarified cell lysate was mixed with IgG Sepharose 6 Fast Flow beads (GE Healthcare) and rotated at 4°C for 1 hr. Beads were washed 5 times with TAP lysis buffer and then once with kinase buffer (50 HEPES [pH 7.4], 150 mM NaCl, 5 mM MgCl2). To assay Fus3 kinase activity, Fus3-TAP kinase assay beads were resuspended in a kinase reaction mix (50 mM HEPES [pH 7.4], 150 mM NaCl, 5 mM MgCl2, 500 once with kinase buγ-^{32}P-ATP; Perkin Elmer) and 0.15 mg/ml MBP). Reactions were stopped after 25 min and analyzed by 12% SDS-PAGE. Fus3-TAP concentration in reactions was determined by immunoblotting with c-Myc antibody (sc-789, Santa Cruz Biotechnology).

Analysis of FRAP Experiments

We used Fluorescence Recovery After Photobleaching (FRAP) to estimate the fraction of Far1 that is fixed in the cytoplasm and the fraction that is rapidly shuttling between the nuclear and cytoplasmic compartments. A confocal microscope was used to measure nuclear and cytoplasmic fluorescence intensity, *Nuc(t)* and *Cyt(t)* respectively (see Materials and Methods; Figures 2A and 2B). To estimate initial nuclear and cytoplasmic fluorescence, N_0 and C_0, we use the first 5 time points, before photobleaching (PB), which are at nearly constant fluorescence. After a small initial reduction due to PB, the cytoplasmic fluorescence, *Cyt(t)*, was nearly constant during the recovery period. The dataset consists of 58 cells of which 29 were treated with saturating αF (760 nM) between 30 and 80 min before imaging. Nuclear Far1-Venus concentration from the FRAP experiments was fitted for each cell to an exponential model, $A - B\, e^{-t/\tau}$, where A and B are constants and t is time (Figure 2B). The time constant for recovery, τ = 4.7 ± 2.3 s (mean ± StdDev), was not affected by pheromone treatment (Figure S3A; p = 0.96), while pheromone decreased the ratio of nuclear to cytoplasmic fluorescence (Figure S3B; $p < 10^{-4}$). For each cell, we normalized our data to the initial nuclear to cytoplasmic fluorescence ratio N_0/C_0. Normalized *Nuc(t)/Cyt(t)* traces for nearly all the cells (52 of 58) reached a steady-state level less than one (Figure 2D), which suggests the presence of a pool of molecules that does not shuttle on the rapid timescale. If all the fluorescence came from rapidly shuttling Far1 molecules, then the steady-state nuclear fraction should not change after PB. This is because PB is expected to reduce the number of visible fluorescent molecules, but not alter their cellular distribution after rapidly shuttling redistributes the remaining fluorescent molecules. Consistent with this interpretation, we see that cells expressing YFP alone (not fused to any protein) recover a normalized steady-state value for normalized *Nuc/Cyt* ratio not significantly different from one (Figure 2D).

To understand the implications of the normalized *Nuc/Cyt* ratio recovering to a level lower than one, we formulated a simple model. The confocal microscope eliminates out of focus illumination so that fluorophore concentration is measured. We expect the initial nuclear and cytoplasmic fluorescence to be given by

$$N_0 = \frac{\gamma(F_n + S_n)}{V_n}, \text{ and } C_0 = \frac{\gamma(F_c + S_c)}{V_c}, \qquad \text{(Equation 1)}$$

where F_n and F_c are the amount of fixed (non-shuttling) nuclear and cytoplasmic Far1-Venus proteins respectively, S_n and S_c are the shuttling nuclear and cytoplasmic Far1-Venus proteins respectively, V_n and V_c are the nuclear and cytoplasmic volume respectively, and γ is the constant that relates fluorophore concentration to measured fluorescence. The total amount of shuttling protein, S_{tot}, is related to its nuclear and cytoplasmic fractions by ϕ so that

$$S_n = \phi S_{tot}, \text{ and } S_c = (1 - \phi) S_{tot}. \qquad \text{(Equation 2)}$$

Combining Equations 1 and 2 yields the initial nuclear to cytoplasm fluorescence ratio

$$\frac{N_0}{C_0} = \frac{V_c}{V_n} \frac{F_n + \phi\, S_{tot}}{F_c + (1 - \phi)\, S_{tot}}. \qquad \text{(Equation 3)}$$

Taking the photobleaching ratio for the nucleus and cytoplasm to be PB_n and PB_c respectively, and assuming that the photobleaching rate is the same for both shuttling and fixed fractions, the amount of shuttling fluorescent molecules remaining after PB, fS_{tot}, will be given by

$$fS_{tot} = (1 - PB_c)\, S_c + (1 - PB_n) S_n = S_{tot}(1 - \phi PB_n - (1 - \phi) PB_c). \qquad \text{(Equation 4)}$$

After PB, the final nuclear and cytoplasmic fluorescence will equilibrate to

$$Nuc(t \to \infty) = \gamma\, (F_n(1 - PB_n) + fS_{tot}\phi)/V_n,$$

$$Cyt(t \to \infty) = \gamma(F_c(1 - PB_c) + fS_{tot}(1 - \phi))/V_c. \qquad \text{(Equation 5)}$$

Combining Equations 3, 4, and 5 we can write an expression for the normalized nuclear to cytoplasmic fluorescence ratio at steady state as

$$\frac{Nuc(t \to \infty)/Cyt(t \to \infty)}{N_0/C_0} = \frac{(F_c + fS_{tot}(1 - \phi))F_n(1 - PB_n) + fS_{tot}\phi(1 - \phi\, PB_n - PB_c(1 - \phi))}{(F_n + \phi\, fS_{tot})F_c(1 - PB_c) + fS_{tot}(1 - \phi)(1 - \phi\, PB_n - (1 - \phi)PB_c)}. \qquad \text{(Equation 6)}$$

The dynamics of the recovery of nuclear fluorescence were not affected by the presence of pheromone (Figure S3A) even though exposure pheromone increased the amount of cytoplasmic Far1 (Figure S3B) consistent with previous

reports (Blondel et al., 1999). Nuclear and cytoplasmic PB ratios are measured to be PB_n = 0.57 ± 0.07 and PB_c = 0.2 ± 0.1 respectively (see Figure S3C and S2D). To calculate the nuclear fraction of shuttling molecules and the amount of fixed cytoplasmic fluorescence, we use the measured initial and final nuclear-to-cytoplasmic fluorescence ratio N_0/C_0 and $Nuc(t\rightarrow\infty)/Cyt(t\rightarrow\infty)$. In addition, if we assume that the amount of fixed nuclear Far1 is negligible, $F_n << \phi S_{tot}$. This yields:

$$\frac{F_c}{S_{tot}} = \frac{\left(1-\frac{Nuc(t\rightarrow\infty)/Cyt(t\rightarrow\infty)}{N_0/C_0}\right)\left(\frac{\frac{V_c}{V_n}(1-PB_c)}{N_0/C_0}+(1-PB_n)\right)}{\left(\frac{Nuc(t\rightarrow\infty)/Cyt(t\rightarrow\infty)}{\frac{V_c}{V_n}}+1\right)(PB_n-PB_c)}, \quad \text{(Equation 7)}$$

$$\phi = 1-\frac{\left(\frac{Nuc(t\rightarrow\infty)/Cyt(t\rightarrow\infty)}{N_0/C_0}\right)(1-PB_c)-(1-PB_n)}{\left(\frac{Nuc(t\rightarrow\infty)/Cyt(t\rightarrow\infty)}{\frac{V_c}{V_n}}+1\right)(PB_n-PB_c)}. \quad \text{(Equation 8)}$$

We measured the ratio of cytoplasmic to nuclear volume, V_c/V_n = 27 ± 14 (Mean ± StdDev) and found no significant differences between pheromone treated and untreated cells (p = 0.43). Using Equations 7 and 8, we calculated the ratio of the fixed cytoplasmic Far1 to the shuttling Far1, F_c/S_{tot}, and the nuclear fraction of shuttling Far1 molecules, ϕ, for each cell using our single cell measurements for PB_n, PB_c, V_c/V_n, N_0/C_0, and $Nuc(t\rightarrow\infty)/Cyt(t\rightarrow\infty)$ (Figure S3E and S3F). Pheromone increases the amount of cytoplasmic non-shuttling Far1-Venus ($p < 0.02$), and pheromone does not significantly modify the nuclear fraction of the shuttling molecules (p = 0.23). We note that the assumption of little fixed Far1 in the nucleus may not be correct, but this does not affect our analysis below identifying the presence of a fixed cytoplasmic pool.

The above analysis shows there is a fixed fraction of Far1-Venus molecules that has no nuclear-cytoplasmic shuttling, but gives no information about the localization of this fixed fraction. To show that there is a cytoplasmic fixed fraction, we decided to do a series of FRAPs in tandem, on the same cells. While the first photobleaching event bleaches both the fixed-nuclear and the shuttling Far1 pools, subsequent photobleaching events are predicted to bleach the shuttling pool of Far1 molecules, but not the pool of cytoplasmic fixed molecules. The analysis is slightly complicated by the fact that we have some unavoidable cytoplasmic bleaching when we photobleach the nucleus. From Equation 4 we can see that the amount of shuttling molecules after the i^{th} photobleaching event is given by

$$fS_{tot,i} = S_{tot}(1-\phi PB_n-(1-\phi)PB_c)^i. \quad \text{(Equation 9)}$$

Note that this assumes we waited for the system to reach steady state before the next bleaching event. In a similar way the final fixed cytoplasmic fluorescence after the i^{th} photobleaching event is given by

$$fF_{C,i} = F_C(1-PB_c)^i. \quad \text{(Equation 10)}$$

Therefore the cytoplasmic fluorescence after the i^{th} photobleaching event is given by

$$Cyt_i = \frac{\gamma}{V_c}\left(F_c(1-PB_c)^i + S_{tot}(1-\phi)(1-\phi PB_n-(1-\phi)PB_C)^i\right). \quad \text{(Equation 11)}$$

If there is no fixed cytoplasmic fluorescence (F_C = 0), the logarithm of the cytoplasmic fluorescence should decrease linearly with the number of FRAPs so that

$$Log_{10}(Cyt_i) = Log_{10}\left(\frac{\gamma S_{tot}(1-\phi)}{V_c}\right) + i\,Log_{10}(1-\phi PB_n-(1-\phi)PB_C), \quad \text{(Equation 12)}$$

where Cyt_i is the cytoplasmic fluorescence upon reaching steady state after the i^{th} photobleaching event. We therefore interpret departures from linearity as evidence of a fixed cytoplasmic fluorescence pool. This departure from linearity can be seen for Far1-Venus (Figure 2E, inset), but not for YFP (Figure 2F, inset). These data support the presence of a fixed pool of Far1 in the cytoplasm.

Far1-Fluorescent Protein Signal-to-Noise Ratio

To calculate the signal-to-noise ratio for the intergenerational memory experiment, a yeast strain with untagged Far1 (AD1-6b) was imaged as Far1-Venus and Far1-GFP. Images were exported and cells were segmented and tracked with identical parameters for tagged and untagged Far1 strains. We define inherited Far1 as the concentration in the daughter cell above and beyond what we estimate that concentration would be in the absence of pheromone. There is still detectable Far1 protein in the absence of pheromone, which we define as the base level for each cell (see main methods). Then the inherited Far1 is taken to be (Far1-base level)/base level. This base level is typically lower than the daughter Far1 level at birth, but not always, because some cells have only been exposed to pheromone for a short time before the daughter cell is born. The base level has the lowest signal-to-noise ratio among any of our fluorescent measurements because this is where there is the lowest amount of Far1-Venus. Therefore, the signal-to-noise calculations that we report here correspond to a lower bound.

To determine signal-to-noise ratios, we first calculated the mean signal and SD for unlabeled cells, i.e., background cell autofluorescence, $\left(S^{GFP/Venus}_{Backgr.}, \sigma^{GFP/Venus}_{Backgr.}\right)$, and for *FAR1-Venus* and *FAR1-GFP* cells, $\left(S^{GFP}_{FAR1-12xL92P,H7\ or\ PEST}, \sigma^{GFP}_{12xFAR1-L92P,H7\ or\ PEST}\right)$ and $\left(S^{Venus}_{WT,CLB5-NES}, \sigma^{Venus}_{WT,CLB5-NES}\right)$.

Next, we subtracted background autofluorescence from the fluorescent signal obtained from Far1-Venus and Far1-GFP signals: $S = S_{fluorescent} - S_{backgr.}$, with a variance of $\sigma^2 = \sigma^2_{fluorescent} + \sigma^2_{backgr.}$. The ratio of this signal value and the variance gives the signal-to-noise ratio for a single time-point. However, since we are averaging multiple time-points in a time-series to determine the base level, the signal-to-noise in our measurements is higher. Specifically, if we assume that:

(i) The signal and noise are uncorrelated,
(ii) Signal strength is approximately constant during the period we are considering
(iii) Noise has constant variance throughout the experiment.

The signal-to-noise ratio in our measurement of base level is given by:

$$\left(\frac{S}{\sigma^2}\right)_{time-series} = \sqrt{n}\,\frac{S}{\sigma},$$

where n is the number of time-points (Drongelen, 2008). In our case, we typically average 10-40 time-points to determine the base level. By using the most conservative value of 10 time-points, we find the following lower bounds for signal-to-noise ratios in different strains (for N cells).

Strain	Mean signal to noise ratio	N
FAR1-Venus	11.4 ± 0.5	33
CLB5-NES FAR1-Venus	11.6 ± 0.6	33
12XFAR1-L92P-GFP	11.2 ± 0.7	25
FAR1-H7-GFP	5.4 ± 0.5	33
FAR1-CLN2-PEST-GFP	6.3 ± 0.6	52

Calculation of Amount of Far1 in Nucleus and Cytoplasm

Using Epifluorescence Imaging

To calculate the relative amount of nuclear and cytoplasmic Far1-Venus, we first arrested cells in 3 nM for 2 hr, and exposed cells for 300 ms using the Colibri 505 LED module at 25% power. Only cells that remained arrested in G1 were used for the analysis. We detected the nucleus using a 2D-Gaussian fit. Nuclear and cell volumes were then calculated using rotational symmetry and background fluorescence was subtracted. This analysis estimated the nuclear Far1 to be ~6% of the total, but pheromone-arrested cells are not rotationally symmetric. To account for the irregular shape of pheromone-arrested cells, we used a simple threshold of fluorescence to segment the nuclei, which resulted in an estimate that 9% of total Far1 was nuclear (see Figures S6A and S6B).

Using Confocal Imaging

As an estimate of the total fraction of cytoplasmic Far1 (i.e., without discriminating among fixed and shuttling molecules), we used the initial fluorescence levels for the nucleus (N_0) and cytoplasm (C_0) of the Far1-Venus strain. The fluorescence signal of the confocal microscope is proportional to the concentration of the fluorophore. We therefore need to take into account the nuclear and cytoplasmic volumes, V_n and V_c respectively, to calculate the total amount of fluorophore. The strain used in this experiment had *WHI5* tagged with mKO, which allowed us to easily identify G1 cells and their nuclei. For each cell we manually fitted an ellipse to the nucleus, as observed in the mKO channel. The nuclear volume was estimated by assuming an ellipsoidal geometry, where the Z-axis was assumed to be equal to the minor axis in the XY plane. In a similar manner we fitted an ellipse to the cell body, based

on the transmission and Venus channels. When present, we fitted an ellipse to the vacuole and to the mating projection. The cytoplasmic volume was then calculated by adding the cell body and mating projection volume, and subtracting the vacuolar and nuclear volumes.

The cytoplasmic fraction of fluorescence was then calculated as

$$CytFrac = \frac{C_0 V_C}{C_0 V_C + N_0 V_N} = \frac{C_0}{C_0 + N_0 \frac{V_N}{V_C}}.$$

Using Nuclear/Cytoplasmic Fractionation

To measure the nuclear and cytoplasmic Far1 using fractionation methods, we followed a protocol modified from (Su et al., 2005). In general, it is challenging to separate the yeast nuclei from the cytoplasm without breaking them, therefore we emphasize that this experiment serves only as a qualitative addition to the quantitative fluorescent experiments presented in Figures S2A–S2C. Yeast cells were grown in 50 ml YPD media until OD600 = 0.35. Cells were then exposed to 240 nM pheromone for 2.5 hr and harvested by centrifugation. Cells were resuspended in 1 ml ice-cold water and centrifuged at 600 g for 5 min at 4°C. Samples were then resuspended in 250 ul (cell pellet volume) of zymolyase buffer I (50 mM Tris-HCl [pH7.5], 10 mM MgCl2, 1M sorbitol, 30 mM DTT), and incubated 15 min at room temperature before centrifugation at 600 g for 5 min at 4°C. The pellet was resuspended in 500 ul zymolyase buffer II (50 mM Tris-HCl [pH7.5], 10 mM MgCl2, 1 M sorbitol, 1 mM DTT + Zymolyase 100T) and incubated at 30°C for 40 min. The spheroplasts were centrifuged down at 200 g at 4°C and washed twice with cold wash buffer (50 mM HEPES-KOH [pH7.5], 20 mM KCl, 2 mM EDTA, 1 M sorbitol, 1 mM PMSF). The pellet was resuspended in 500 ul of lysis buffer A (10 mM HEPES [pH7.9], 10 mM KCl, 1.5 mM MgCl, 0.1 mM EDTA, 0.5 mM DTT, 0.4% NP-40, 1 mM PMSF, complete protease inhibitor cocktail). Cells were spun down gently at 4°C and supernatant was collected as cytoplasm. The rest of the pellet was resuspended in 50 ul of lysis buffer B (20 mM HEPES [pH7.9], 420 mM NaCl, 1.5 mM MgCl2, 25% glycerol, 1 mM PMSF, 0.2 mM EDTA, 0.5 mM DTT, complete protease inhibitor cocktail), incubated on ice for 10 min, and then vortexed for 1 min. Samples were clarified by centrifugation at 16000 g for 10 min at 4°C and the supernatant was collected as nuclear extract. Proteins from the fractions were resolved by 8% SDS-PAGE and blotting was performed using semidry blotter (Bio-Rad). The antibody used for detection of Far1-3HA was HA.11 clone 16B12 (Covance). The gel was quantified using ImageJ software and band intensities correspond to the same amount of loaded protein.

Using Immunofluorescence

Following (Amberg et al., 2005a), cells were grown in SCD media to early exponential phase and then arrested with either 240 nM or 3 nM pheromone. Cells were fixed with formaldehyde (concentration 3.7%) for 1 hr at room temperature. Cells were then washed twice with 0.1 M potassium phosphate (pH 7.5) and once with 1.2 M sorbitol. Cells were then treated with zymolyase and spheroplasts were harvested by centrifugation and washed one more time with PBS. Cells were spotted onto polylysine coated slides and these slides were then immersed for 5 min in methanol (pre-cooled to −20°C) and for 30 s in acetone (room temperature). Cells were blocked (PBS + 3% BSA) for 1 hr and then incubated with the primary antibody (HA.11 clone 16B12 1:500, Covance), washed and incubated with secondary antibody conjugated with Texas Red (1:500, Life Technologies). After washes, cells were covered with SlowFade Gold antifade reagent (Life Technologies), and imaged. Nuclei were identified using DAPI stain and segmented.

Calculations of Time from Peak to Half-Maximum Cytoplasmic Far1

In the main Figures 1D, and 4C, and 5C we are currently using the (total) concentration to calculate the time from peak to half-maximum cytoplasmic Far1. Using the total concentration of Far1 is warranted because the starting point for our half-maximum measurement is *Start* when most nuclear Far1 is degraded. Moreover, most of the Far1 is cytoplasmic as shown in the above analysis. However, to control for possible artifacts related to this measurement we also calculated the same time to half maximum using the cytoplasmic Far1 only (the nucleus was detected using a 2D-Gaussian and its fluorescence was subtracted). The results show no significant difference between these measurements (see Figures S5A and S5B).

Measurement Showing that Far1-Localization Does Not Affect Far1 Expression

To test whether altered Far1 localization affects its expression levels, we arrested strains expressing Far1-GFP (wt) and Far1-NES-GFP in 3 nM α-factor. Cells were segmented, tracked, and the fluorescent signals were measured. To compare expression levels, we next quantified the increase (measured by fluorescence intensity) for the first 30 min of arrest for each strain. To control for possible effects due to cell size (WT and Far1-NES-GFP have slightly different cell size distributions), we plotted the Far1 increase as a function of cell volume for these two strains (see Figure S1D). No significant difference was observed.

Chemotropism Assay in Microfluidic Devices

Chemotropism assays were performed as described in (Ventura et al., 2014). Briefly, we fabricated microfluidic devices designed for the generation of stable gradients in open chambers using standard protocols for polydimethylsiloxane (PDMS)

Table S1. List of Strains

Name	Genotype	Source
AD1-6b	*MAT**a** bar1::URA3 trp1::TRP1-MET3pr-CLN2 WHI5-mCherry-spHIS5*	This study
AD2-8c	*MAT**a** bar1::URA3 trp1::TRP1-MET3pr-CLN2 WHI5-mCherry-spHIS5 FAR1-Venus-kanMX ADE2*	(Doncic and Skotheim, 2013)
AD5-17d	*MAT**a** bar1::URA3 trp1::TRP1-MET3pr-CLN2 WHI5-mCherry-spHIS5 FAR1-Venus-kanMX ADE2 cln1::HIS3 cln2Δ*	(Doncic and Skotheim, 2013)
AD18-5	*MAT**a** bar1::URA3 WHI5-mCherry-spHIS5, ADE2, far1Δ::TRP1-GAL1pr-FAR1-Venus-kanMX*	(Doncic and Skotheim, 2013)
AD19-36d	*MAT**a** bar1::Nat WHI5-mCherry-SpHIS5 ADE2 FAR1-Venus-kanMX trp1::TRP1-MET3pr-CLN2 clb5::URA3 clb6::LEU2*	(Doncic and Skotheim, 2013)
AD21-19a	*MAT**a** bar1::Nat CLN2-NES-URA3 trp1::TRP1-MET3pr-CLN2 cln2::LEU2 MYO1-GFP-kanMX WHI5-GFP-kanMX, HTB2-mCherry-spHIS5 cln1Δ*	This study
AD27-3	*MAT**a** bar1::Nat CLN2-NLS-URA3 HTB2-mCherry-SpHIS5 trp1::TRP1-MET3pr-CLN2 WHI5-GFP-kanMX cln1Δcln2Δ*	This study
AD28-5	*MAT**a** bar1::URA3 WHI5-mCherry-spHIS5 ADE2 trp1::TRP1-MET3pr-CLN2 FAR1-GFP-NES-kanMX*	This study
AD34-6	*MAT**a** bar1::URA3 WHI5-mCherry-spHIS5 ADE2 FAR1-Venus-kanMX trp1::TRP1-MET3pr-CLN2 CLB5-NES-Nat*	This study
AD36-1	*MAT**a** bar1Δ, FAR1-GFP-TRP1, WHI5-mKoκ-LEU2, bni1::kanMX*	This study
FUS3-GFP	*MAT**a** FUS3-GFP*	(Ghaemmaghami et al., 2003)
OA003	*MAT**a** bar1Δ FAR1-GFP-TRP1*	This study
OA040	*MAT**a** bar1::URA3 WHI5-mKoκ-TRP1 far1::kanMX-FAR1pr-FAR1-GFP-LEU2 ADE2*	This study
OA041	*MAT**a** bar1::URA3 WHI5-mKoκ-TRP1 far1::kanMX-FAR1pr-FAR1(L92P)-GFP-LEU2 ADE2*	This study
OA042	*MAT**a** bar1::URA3 WHI5-mKoκ-TRP1 far1::kanMX-12xFAR1pr-FAR1(L92P)-GFP-LEU2 ADE2*	This study
OA050	*MAT**a** bar1::URA3 WHI5-mKoκ-TRP1 far1::kanMX-spHIS5-GAL1pr-FAR1(L92P)-GFP-LEU2 ADE2*	This study
OA056	*MAT**a** bar1::URA3 WHI5-mKoκ-TRP1 far1::kanMX-FAR1pr-FAR1(H7)-GFP-LEU2 ADE2*	This study
OA057	*MAT**a** bar1::URA3 WHI5-mKoκ-TRP1 far1::kanMX-FAR1pr-FAR1(D1A)-GFP-LEU2 ADE2*	This study
OA058	*MAT**a** bar1::URA3 WHI5-mKoκ-TRP1 far1::kanMX-FAR1pr-FAR1-GFP-CLN2PEST-LEU2 ADE2*	This study
OA059	*MAT**a** bar1::URA3 WHI5-mKoκ-TRP1 far1::kanMX-HIS-GAL1pr-FAR1(H7)-GFP-LEU2 ADE2*	This study
OA062	*MAT**a** bar1::URA3 WHI5-mKoκ-TRP1 far1::kanMX-HIS-GAL1pr-FAR1(D1A)-GFP-LEU2 ADE2*	This study
OA063	*MAT**a** bar1::URA3 WHI5-mKoκ-TRP1 far1::kanMX-HIS-GAL1pr-FAR1-GFP-CLN2PEST-LEU2 ADE2*	This study
TCY3057	*MAT**a** bar1Δ ste5::STE5-YFP trp1::STE5pr-YFP-STE5-TRP1*	(Yu et al., 2008)
YAG5040	*MAT**a** bar1::URA3 WHI5-mKO-spHIS5 ADE2 far1Δ::TRP1-GAL1pr-FAR1-Venus-kanMX*	This study
TCY3154	*MAT**a** bar1Δ ACT1::ACT1pr-CFP-TRP1 PRM1::PRM1pr-YFP-HIS5 CDC28-F88A*	(Colman-Lerner et al., 2005)

microfluidic device construction (Keenan et al., 2006). A device pre-treated with poly-D-lysine (1mg/ml, Sigma) and concanavalin A (1mg/ml, Sigma) was filled with 0.22μm-filtered synthetic complete medium alone or with 175 nM αF and 0.1 mg/ml bromophenol blue (BPB) as tracking dye. All media contained 100 ppm PEG3000 (Sigma) to prevent nonspecific αF binding to the container's surfaces. After confirming the correct formation of the gradient by monitoring BPB fluorescence, we stopped the flow, washed the chambers with media, and loaded a sonicated yeast exponential culture on top of the device. In each experiment, we use a culture containing a 1:1 mix of a control strain (TCY3154), which expresses YFP under the control of pheromone responsive promoter (Colman-Lerner et al., 2005) and the strain whose polarization ability was to be evaluated. We allowed cells to settle and bind to the glass bottom before resuming flow. We performed imaging over 4 hr using an Olympus IX-81 microscope, with an Olympus UplanSapo objective with a magnification of 63 × (N.A. = 1.35) coupled with an HQ2 (Roper Scientific) cooled CCD camera. The angle of polarization was manually measured using ImageJ after 4 hr in both gradient and isotropic chambers: zero degrees correspond to perfect alignment with the gradient and 180 degrees correspond to growth in the opposite direction.

Table S2. List of Plasmids

Name	Description	Source
pAD5-2	pRS40x *CLB5pr-CLB5-NES-NatMX6*	This study
pOA38	pRS405 *FAR1pr-FAR1-GFP-LEU2*	This study
pOA39	pRS405 *FAR1pr-FAR1-L92P-GFP-LEU2*	This study
pOA43	pRS405 *FAR1pr-FAR1-D1A-GFP-LEU2*	This study
pOA44	pRS405 *FAR1pr-FAR1-GFP-CLN2PEST-LEU2*	This study
pOA45	pRS405 *FAR1pr-FAR1-H7-GFP-LEU2*	This study

All strains except the *FUS3-GFP* strain were obtained by standard methods, are congenic with W303 (leu2-3,112 his3-11,15 ura3-1 trp1-1 can1-1), and were constructed from laboratory stocks. The FUS3-GFP strain was obtained from the genome-wide GFP fusion library (Ghaemmaghami et al., 2003) and has a BY4741 background (*MAT***a** *his3Δ1 leu2Δ0 LYS2 met15Δ0 ura3Δ0*). To construct the *10-12xFAR1-L92P-GFP* strain (OA042), *FAR1pr-FAR1-L92P-GFP*, with the linker between *FAR1* and *GFP* used in (Longtine et al., 1998), was assembled on an pRS405 integrating plasmid, which was then cut with the restriction enzyme AvrII and transformed into the *FAR1* promoter region of a *far1Δ* deletion strain using standard methods (Amberg et al., 2005b). We used qPCR to determine the copy number of integrants. The genomic location of *FAR1-L92P* insertion was verified to be at Far1 promoter by PCR. We were able to get high copies of integrants because cut integrating plasmids frequently result in multiple, tandem integrations (Orr-Weaver and Szostak, 1983). About 50% of colonies were found to harbor single copy Far1-L92P (OA041) while 15%–20% of colonies had >3 copies of Far1-L92P (OA042 had 10-12 copies). To construct *FAR1-D1A-GFP* (G646D) and *FAR1-H7-GFP* (K757STOP) strains (Nern and Arkowitz, 2000), *FAR1pr-FAR1-GFP* was first assembled on a pRS405 integrating plasmid (pOA38). This plasmid was then modified by QuikChange Site-Directed Mutagenesis XL Kit (Qiagen) to generate *FAR1pr-FAR1-D1A-GFP*. *FAR1pr-FAR1-H7-GFP* plasmids were made by digesting pOA38 with PacI and NheI and religating using complementary primers. These plasmids were verified by sequencing and integrated into the *FAR1* promoter region of a *far1Δ* deletion strain. Single integration was verified by qPCR, sequencing, fluorescence microscopy, and size distribution (Coulter-Counter) measurements.

Plasmids were constructed using standard methods. pAD5-2 was made from a pRS40x backbone, where the selectable marker was changed to NatMX by Chris Aakre. 808bp of the *CLB5* promoter is followed by the *CLB5* gene fused to a nuclear export sequence from PKI, LALKLAGLDI (Wen et al., 1995). This was integrated to create strain AD34-6 after restriction digest by StuI.

SUPPLEMENTAL REFERENCES

Amberg, D.C., Burke, D., and Strathern, J.N.; Cold Spring Harbor Laboratory (2005a). Methods in yeast genetics: a Cold Spring Harbor Laboratory course manual, 2005 edn (Cold Spring Harbor, N.Y.: Cold Spring Harbor Laboratory Press).

Amberg, D.C., Burke, D.J., and Strathern, J.N. (2005b). Methods in Yeast Genetics: A Cold Spring Harbor Laboratory Course Manual (CSHL Press).

Drongelen, W. (2008). Signal Processing for Neuroscientists (Academic Press).

Ghaemmaghami, S., Huh, W.K., Bower, K., Howson, R.W., Belle, A., Dephoure, N., O'Shea, E.K., and Weissman, J.S. (2003). Global analysis of protein expression in yeast. Nature *425*, 737–741.

Jorgensen, P., Edgington, N.P., Schneider, B.L., Rupes, I., Tyers, M., and Futcher, B. (2007). The size of the nucleus increases as yeast cells grow. Mol. Biol. Cell *18*, 3523–3532.

Keenan, T.M., Hsu, C.H., and Folch, A. (2006). Microfluidic "jets" for generating steady-state gradients of soluble molecules on open surfaces. Appl. Phys. Lett. *89*, 114103.

Longtine, M.S., McKenzie, A., 3rd, Demarini, D.J., Shah, N.G., Wach, A., Brachat, A., Philippsen, P., and Pringle, J.R. (1998). Additional modules for versatile and economical PCR-based gene deletion and modification in Saccharomyces cerevisiae. Yeast *14*, 953–961.

Orr-Weaver, T.L., and Szostak, J.W. (1983). Multiple, tandem plasmid integration in Saccharomyces cerevisiae. Mol. Cell. Biol. *3*, 747–749.

Su, H., Bidère, N., Zheng, L., Cubre, A., Sakai, K., Dale, J., Salmena, L., Hakem, R., Straus, S., and Lenardo, M. (2005). Requirement for caspase-8 in NF-kappaB activation by antigen receptor. Science *307*, 1465–1468.

Ventura, A.C., Bush, A., Vasen, G., Goldín, M.A., Burkinshaw, B., Bhattacharjee, N., Folch, A., Brent, R., Chernomoretz, A., and Colman-Lerner, A. (2014). Utilization of extracellular information before ligand-receptor binding reaches equilibrium expands and shifts the input dynamic range. Proc. Natl. Acad. Sci. USA *111*, E3860–E3869.

Wen, W., Meinkoth, J.L., Tsien, R.Y., and Taylor, S.S. (1995). Identification of a signal for rapid export of proteins from the nucleus. Cell *82*, 463–473.

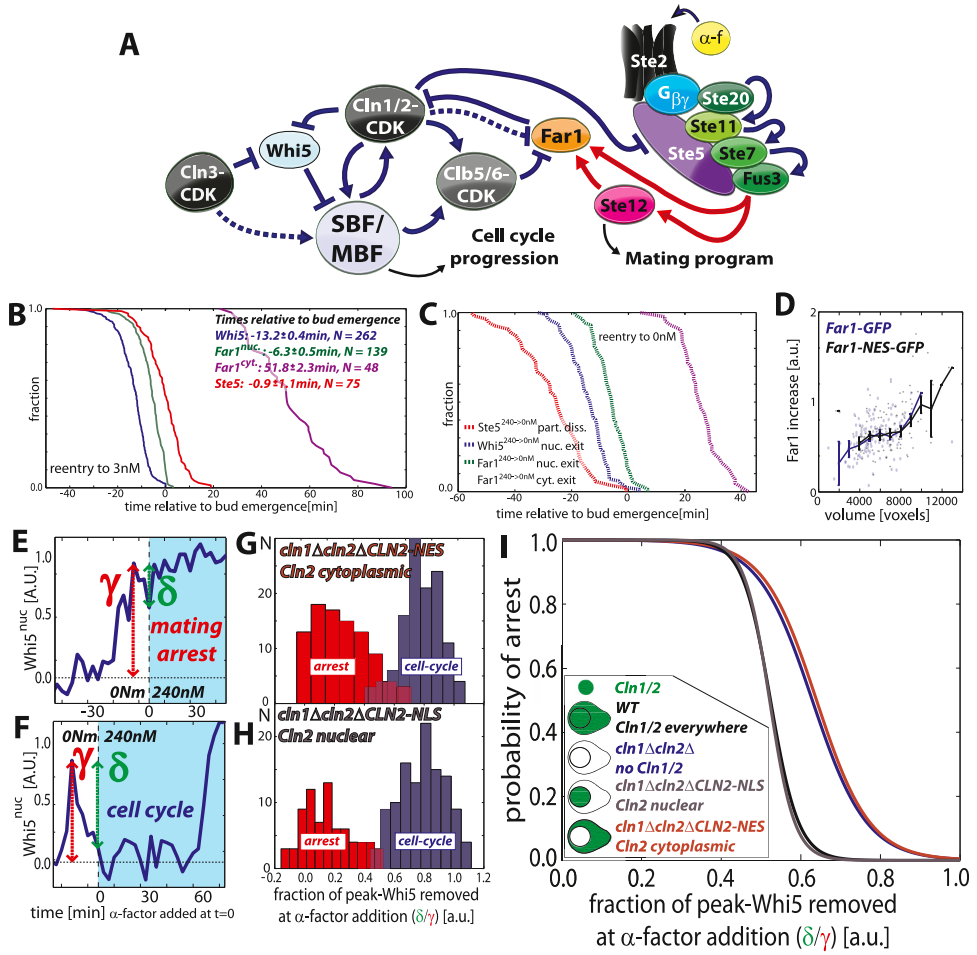

Figure S1. Cytoplasmic Far1 Is Inherited to Provide Intergenerational Memory across the Start Switch, Related to Figure 1

(A) Schematic of cell-cycle-mating pathway interactions in budding yeast.

(B and C) Time to reach half-maximum concentrations relative to bud emergence was measured using strains containing Whi5-mCherry, Far1-Venus, Ste5-YFP in cells that are initially arrested in 240 nM α-factor and then released to 3 nM (B) or 0 nM (C) α-factor. Note that for the 3 nM experiment, the Ste5-YFP timing is for partial disassociation (see main text for details).

(D) Altered localization does not affect Far1 expression. *WT* and *FAR1-NES* cells were arrested in 3 nM α-factor and the increase of Far1-GFP was measured as described in the methods above; N_{WT} = 119, $N_{FAR1\text{-}NES}$ = 115.

(E and F) Example cell traces of nuclear Whi5-GFP used in the commitment assay described in (Doncic et al., 2011). The relative amount of nuclear Whi5-GFP at the time of mating pheromone exposure and subsequent cell fates were measured.

(G and H) Histograms of relative amounts of exported nuclear Whi5-GFP at the time of pheromone addition and cell fate (arrest or divide) for *CLN2-NES* and *CLN2-NLS* strains.

(I) Estimated probability of having committed to division given a measurement of nuclear Whi5-GFP for *WT*, *cln1Δcln2Δ*, *CLN2-NES* and *CLN2-NLS* strains. Cells with nuclear Cln2 commit as WT and cells with cytoplasmic Cln2 commit as *cln1Δcln2Δ* suggesting that the decision to commit is mediated by the nuclear pool of Cln2. WT and *cln1Δcln2Δ* data are from (Doncic et al., 2011); $N_{CLN2\text{-}NLS}$ = 189 and $N_{CLN2\text{-}NES}$ = 211.

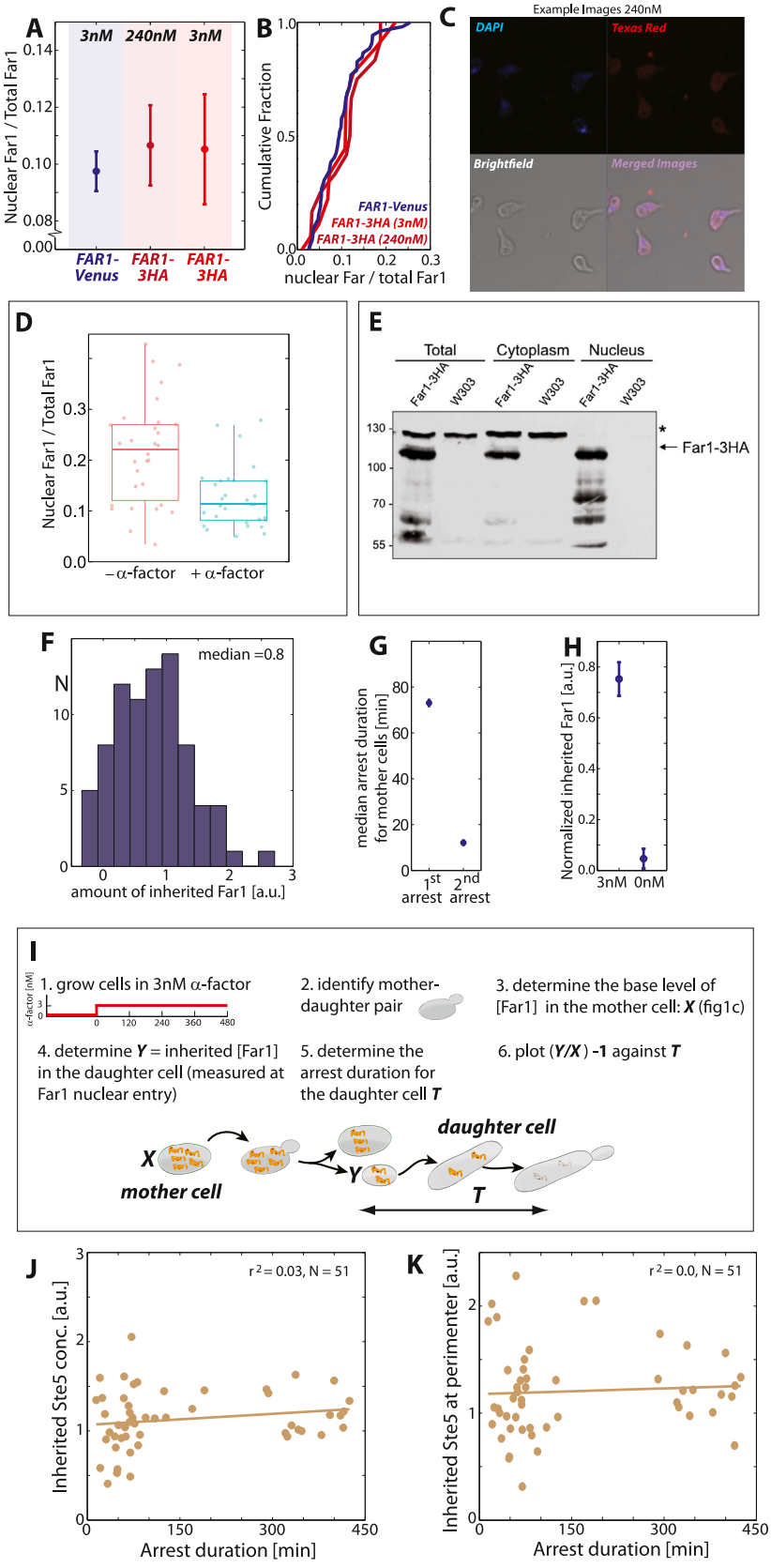

(legend on next page)

Figure S2. Far1 Is Inherited across Generations, Related to Figure 1

(A and B) The fraction of Far1 that is nuclear was estimated using widefield microscopy of *FAR1-Venus* cells (blue), and immunofluorescence (red; see methods above) for *FAR1-3HA* cells after a 2 hr arrest in 3 nM or 240 nM α-factor. Means plotted with associated SE.

(C) Corresponding immunofluorescence images.

(D) Confocal imaging (see methods above) was used to estimate the fraction of nuclear Far1 in the presence (240 nM) or absence of pheromone.

(E) Nuclear and cytoplasmic fractions of Far1 measured using western blot following fractionation (see methods above). The relative band intensity of similarly loaded amounts of protein is shown. We note that since the budding yeast nucleus is ~7% of the total cell volume (Jorgensen et al., 2007), this measurement is roughly consistent with ~10% of Far1 protein being nuclear.

(F)The amount of Far1 inherited by the daughter cell was measured at the time of the mother cell's first cytokinesis (green arrow Figure 1C in main text).

(G) First and second G1-arrest durations were measured for mother cells in 3 nM α-factor confirm that mother cells do not rearrest.

(H) Inherited Far1 for daughter cells in 3 nM and 0 nM pheromone are significantly different ($p < 10^{-4}$). Plotted here are medians ± SEs; $N_{3nM} = 71$, $N_{0nM} = 36$. Note that the value for 0 nM is not significantly different from 0, suggesting that cycling cells does not inherit Far1.

(I) Experimental schematic for the measurement of inherited Far1. We note that we are defining the inherited Far1 as the amount of Far1 in daughter cells above the base level of their mother as measured from previous cell cycles (see methods in main text and signal-to-noise section above).

(J and K) Inherited Ste5 concentration or the amount at the cell perimeter did not correlate with arrest duration.

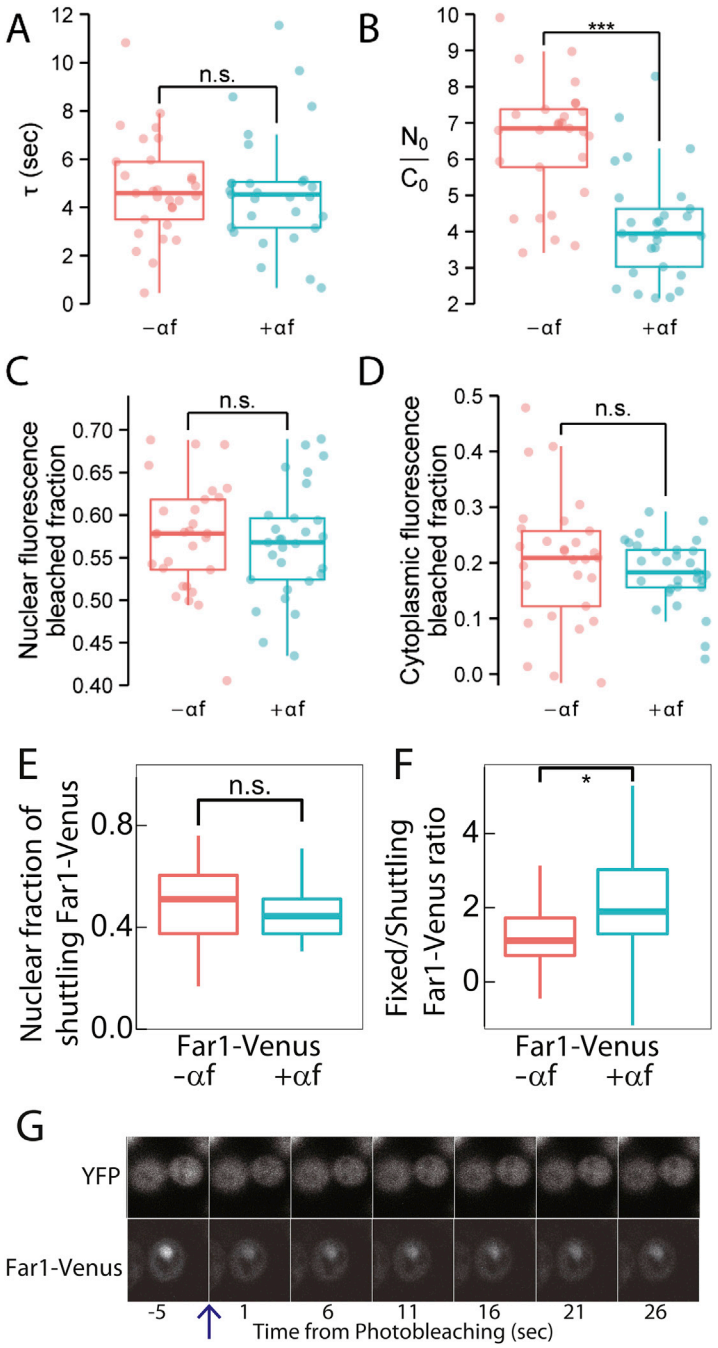

Figure S3. Supporting Figure for FRAP Experiments, Related to Figure 2

(A) Nuclear fluorescence recovery time constant τ from exponential fits to cells bleached in pheromone-free or 760 nM pheromone (±αf) containing medium.

(B) Initial nuclear-to-cytoplasm fluorescence ratio N_0/C_0.

(C) Fraction of nuclear fluorescence photobleached.

(D) Faction of cytoplasmic fluorescence photobleached.

(E) Distribution of the nuclear fraction of the pool of shuttling Far1-Venus for individual cells. See analysis above for a description of our model and estimation procedures.

(F) Distribution of the ratio of fixed to shuttling Far1-Venus fractions for individual cells.

(G) Fluorescence images corresponding to a single FRAP experiment for YFP (above) and Far1-Venus (below).

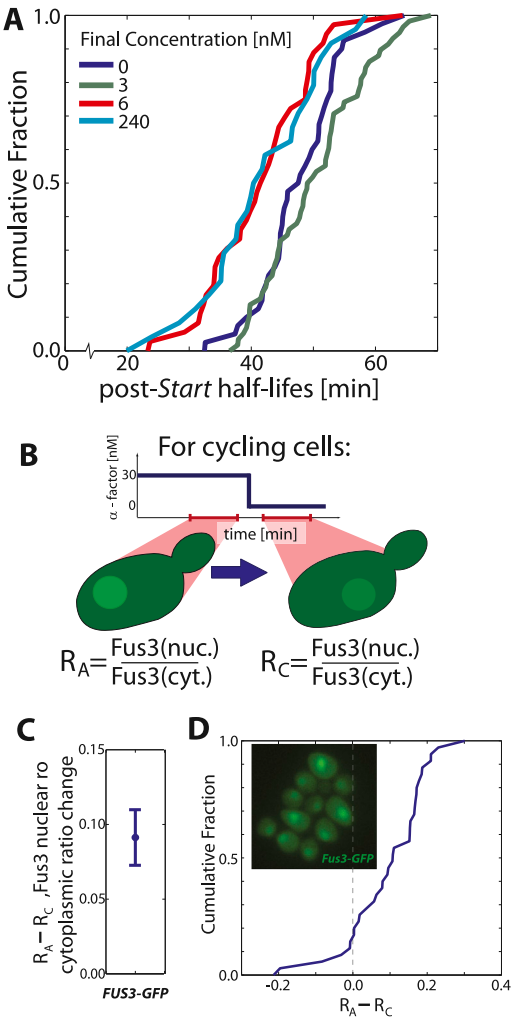

Figure S4. Data Supporting MAPK Activity in S/G2/M, Related to Figure 3

(A) Cumulative distributions for data presented in Figure 3B in the main text.

(B) Schematic for determining pheromone-induced Fus3 localization.

(C) A significantly larger fraction of Fus3 is nuclear in cycling S/G2/M cells in the presence of pheromone ($p < 10^{-4}$, $n = 36$). Note that for this *FUS3-GFP* strain we adjusted the mating pheromone concentration to accommodate for the fact that this strain expresses the pheromone protease Bar1.

(D) Corresponding cumulative distribution of the nuclear ratio difference for Fus3-GFP (example cells shown in inset).

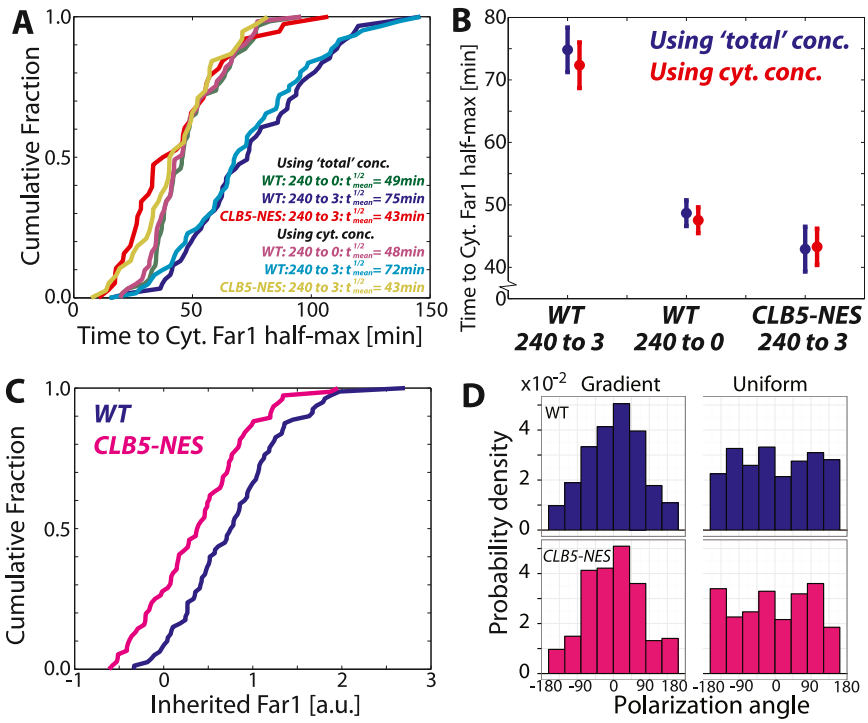

Figure S5. Supporting Data for CLB5-NES Analysis, Related to Figure 4

(A) Cumulative distributions for the time to half-maximum of cytoplasmic Far1 post-*Start* for *WT* and *CLB5-NES* cells corresponding to the data shown in Figures 1D and 4C in the main text; $n_{WT:\ 240\ to\ 0} = 62$, $n_{WT:\ 240\ to\ 3} = 62$ and $n_{CLB5\text{-}NES:\ 240\ to\ 3} = 39$.

(B) Time to Far1 half-maximum was also calculated using only the cytoplasmic fraction of Far1. There is no significant difference compared to examining the time to half-maximum using total Far1 (see methods above; $p > 0.5$ for all comparisons).

(C) Significantly less Far1 was inherited in *CLB5-NES* cells compared to WT ($p < 0.05$).

(D) *CLB5-NES* cells are able to detect the direction of a pheromone gradient as well as WT cells. The gradient detection was performed as in (Ventura et al., 2014). For each cell, the angle between polarization and the direction of the pheromone gradient was measured. The panel shows the estimate of the probability density of these angles for WT (top, blue) and *CLB5-NES* (bottom, pink) cells. The right hand side panels indicates random polarization in the absence of a gradient in our device.

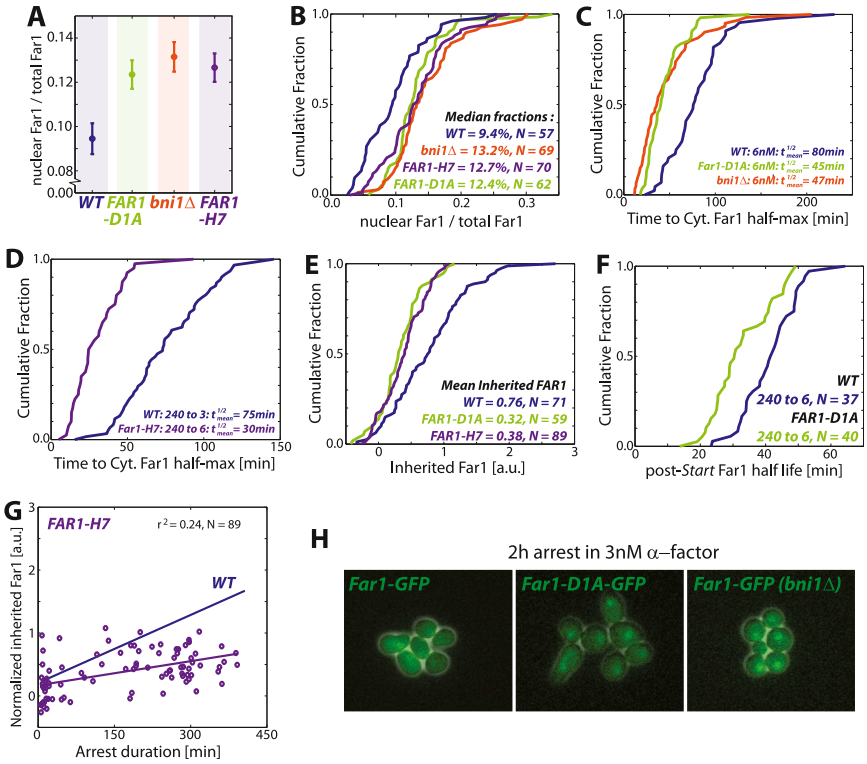

Figure S6. Far1 Binding to Cdc24 Is Required for Intergenerational Memory, Related to Figure 5

(A) Fraction of Far1 that is nuclear for the indicated genotypes as measured using wide field fluorescence microscopy.

(B) Cumulative distributions for data presented in (A).

(C) Time to cytoplasmic half-maximum was calculated as previously described for cells of the indicated genotype exposed to 6 nM. This shows the full distributions corresponding to data presented in Figure 5C.

(D) Time to cytoplasmic half-maximum was calculated as previously described for cells of the indicated genotype exposed first to a 30 min pulse of 240 nM pheromone and then to 6 nM. The slight increase in the time to reach half-maximum Far1 in WT cells shown in (D) compared to (C) is most likely due to increased Far1 expression at 6 nM (Doncic and Skotheim, 2013).

(E) Cumulative distributions for data shown in Figure 5E for mean inherited Far1 for indicated genotypes.

(F) Cumulative distributions for post-*Start* half-life, n = 40. *WT* values from Figure 3B from the main text are shown for comparison.

(G) Intergenerational memory experiment for *FAR1-H7* cells.

(H) Composite phase and fluorescence images for cells of the indicated genotype. *bni1Δ* cells arrest round and with a larger fraction of Far1 in the nucleus.

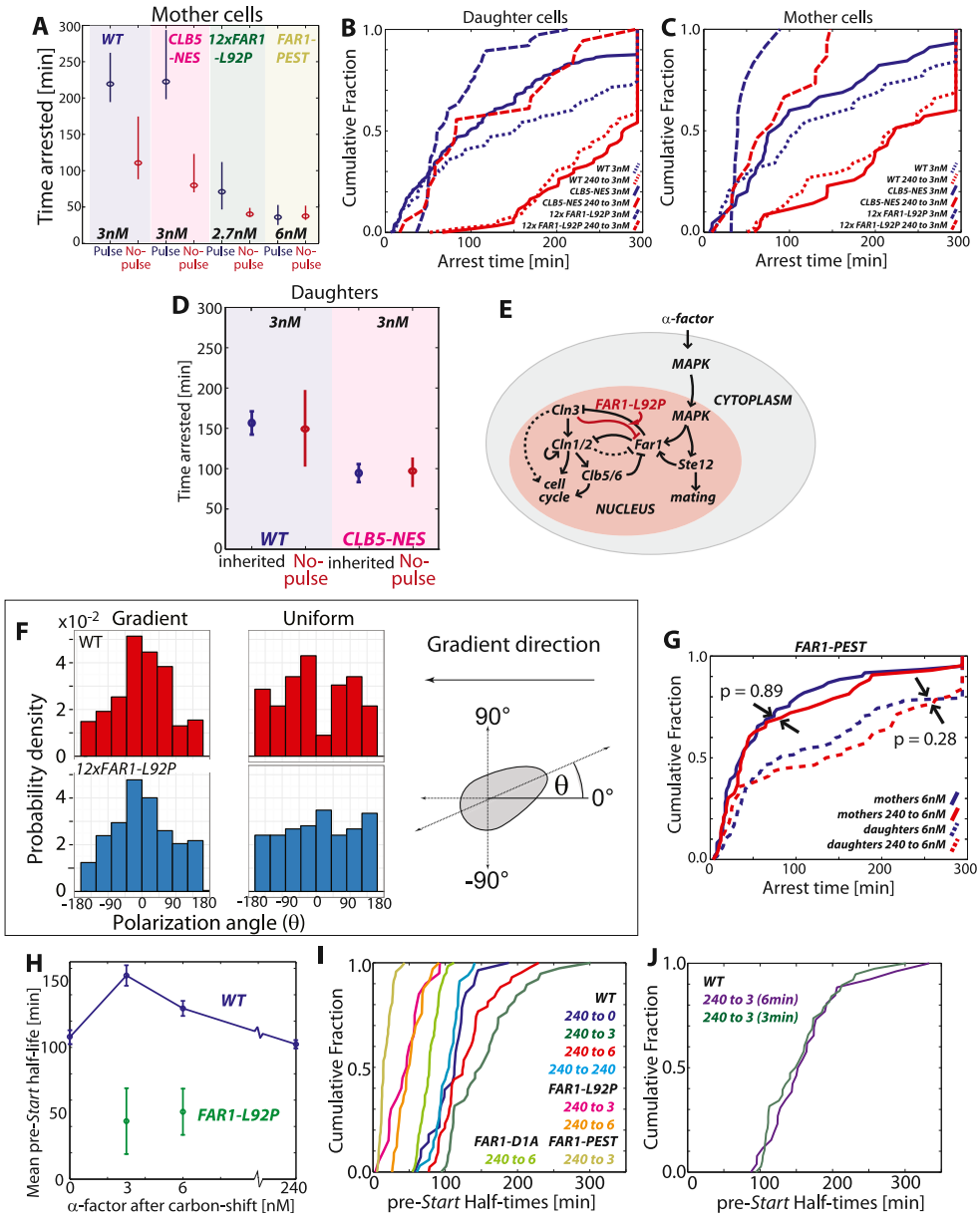

Figure S7. Protein Stability Is Required for Intra- and Inter-Generational Memory, Related to Figure 6

(A) Data for mother cells corresponding to Figure 6B in the main text; From left to right n = 29, 37, 21, 42, 16, 13, 41, and 58.

(B and C) Cumulative distributions for data shown in Figures 6B and S7A.

(D) A comparison of arrest times for the intergenerational experiment (Figure 4F) with the intragenerational experiment without pheromone pulse (Figure 6B) shows no significant difference.

(E) Schematic depicting the proposed mechanism for how the stability of Far1-L92P is decreased (E.V. and M.L., unpublished data).

(F) *12xFAR1-L92P* cells are able to detect the direction of a pheromone gradient as well as WT cells. The gradient detection was performed as in (Ventura et al., 2014). For each cell, the angle between polarization and the direction of the pheromone gradient was measured and the probability density estimated.

(G) Cumulative distributions for the *FAR1-PEST* strain as shown in Figures 6B and S7A.

(H and I) Mean half-lives (H) and cumulative distributions (I) for data shown in Figures 6D and 6G in the main text. From left to right in (I) for WT cells, n = 29, 39, 44, and 35. n = 21 and 43 for *FAR1-L92P* cells in 3 and 6 nM respectively.

(J) To control for possible photobleaching of Venus, we measured the half-life for WT cells using a lower sampling rate (once per 6 min rather than once per 3 min) and calculated the half-life of Far1-Venus in pre-*Start* cells in 3 nM pheromone. No significant difference was found indicating negligible photobleaching under our experimental conditions (p = 0.54).